Research Paper

Targeting PERK-ATF4-P21 axis enhances the sensitivity of osteosarcoma HOS cells to Mppα-PDT

Shenxi Zhong[1,2,*], Ye Zhang[1,2,*], Hai Mou[1,2], Changchun Jian[1,2], Qiu Huang[1,2], Yunsheng Ou[1,2]

[1]Department of Orthopedics, The First Affiliated Hospital of Chongqing Medical University, Yuzhong, Chongqing 400016, China
[2]Orthopedic Laboratory of Chongqing Medical University, Yuzhong, Chongqing 400016, China
[*]Equal contribution and co-first authors

Correspondence to: Yunsheng Ou; **email:** ouyunsheng2001@163.com, https://orcid.org/0000-0001-8578-3523
Keywords: MPPα-PDT, human osteosarcoma, PERK pathway, autophagy, apoptosis, p21
Received: October 10, 2023 **Accepted:** December 29, 2023 **Published:** February 5, 2024

ABSTRACT

Osteosarcoma (OS) is the most prevalent type of malignant bone tumor in adolescents. The overall survival of OS patients has reached a plateau recently. Thus, there is an urgent need to develop approaches to improve the sensitivity of OS to therapies. Pyropheophorbide-α methyl ester-mediated photodynamic therapy (MPPα-PDT) is a new type of tumor therapy, and elucidating its mechanism is helpful to improve its anti-tumor efficacy. Here, we investigated how PERK signaling promotes the human OS (HOS) cell survival induced by MPPα-PDT, as overcoming this may enhance sensitivity to MPPα-PDT. We found that MPPα-PDT combined with PERK inhibitor GSK2656157 enhanced HOS cell apoptosis by suppressing autophagy and p21. Autophagy inhibition and p21 depletion enhanced cell death, indicating pro-survival effects in MPPα-PDT. Notably, p21 was found to be an effector of the PERK-Atf4 pathway, which could positively regulate autophagy mediated by MPPα-PDT. In conclusion, we found that the combination of MPPα-PDT and GSK2656157 enhanced apoptosis in HOS cells by inhibiting autophagy. Mechanistically, this autophagy is p21-dependent and can be suppressed by GSK2656157, thereby enhancing sensitivity to MPPα-PDT.

INTRODUCTION

Osteosarcoma (OS), the most common bone malignancy in adolescents and young adults, is characterized by a high rate of lung metastases [1]. Despite advances in treatment with a combination of chemotherapy and surgery, its 5-year survival rate remains low [2, 3]. Thus, there is an urgent need for more effective OS therapies. Photodynamic therapy (PDT) is a novel anti-tumor approach that relies on photosensitization transferring excited-state energy to cellular oxygen during irradiation at a specific wavelength. Cytotoxic reactive oxygen species (ROS) are produced during this procedure [4, 5]. Pyropheophorbide-α methyl ester (MPPα) is a new type of second-generation photosensitizer that is characterized by its high stability and high concentration in tumors [6]. To date, MPPα-PDT has been shown to possess anti-tumor properties against OS, lung cancer, and breast cancer [7–9]. However, it may also trigger resistance to treatment. In our previous work, we have proved that MPPα-PDT triggers processes including pumping out of intracellular MPPα and ROS, contributing to adaption and even resistance to MPPα-PDT [10, 11].

The endoplasmic reticulum (ER), the production site for secreted or membrane-associated proteins, is a subcellular entity that dynamically reacts to stress signals to control overall protein synthesis. Various

cellular challenges such as ROS, hypoxia, and nutrient deprivation may disrupt ER reduction/oxidation (redox) regulation as well as homeostasis. This may lead to ER stress and an increasing number of misfolded and unfolded proteins, also referred to as the unfolded protein response (UPR) [12]. Physiologically, ER stress is an adaptive response to physiological challenges that promotes cell survival. If the stressor is overly intense or persists for an extended period, the accumulation of unfolded or misfolded proteins in the ER triggers the relevant ER stress signaling pathway, leading to cell apoptosis [13]. The primary modulators and immediate enablers of the ER stress response mechanism include protein kinase RNA-like ER kinase (PERK), eukaryotic initiation factor 2α (eIF2α), activating transcription factor 4 (ATF4), and C/EBP homologous protein (CHOP). When ER stress occurs, GRP78 separates from these proteins and activates their downstream signaling pathways, respectively, to rebuild the functional stability of the ER and enhance the adaptability of cells to adverse stimuli. During this process, PERK forms a dimer and autophosphorylates, generating its active, phosphorylated form. Further phosphorylations modify eIF2α, which inhibits ER mRNA translation and protein synthesis functions. Stress sensors in the ER lumen detect ROS, which in turn intensify UPR signaling [14, 15]. By phosphorylating and stabilizing NRF2, PERK reduces ROS accumulation, which controls the expression of phase II detoxification enzymes induced by ROS, such as glutathione S-transferase and HO-1 [16]. Given that PDT targeting triggers cancer cell death via intracellular ROS generation, the PERK pathway presents a plausible candidate for a resistance mechanism.

Autophagy, a conserved and regulated catabolic process, eliminates cytosolic material such as damaged organelles and long-lived proteins [17]. In specific situations, it may serve as a vital factor contributing to pro-survival adaptive reactions. However, previous studies have presented conflicting evidence on the effects of autophagy on apoptosis, and the functions of autophagy in tumorigenesis and anti-cancer treatments remain paradoxical. Autophagy has been reported to inhibit cell apoptosis and promote tumor survival. However, other studies indicate that autophagy enhances cancer cell sensitivity [18, 19]. Thus, the role and underlying mechanisms of autophagy in cancer treatment require clarification.

In our previous work, we found that MPPα-PDT activated PERK signaling in human OS (HOS) cells, although the mechanism remained unclear [19]. In the present study, the pro-survival role and underlying mechanism of PERK-eIF2α-ATF4-P21 signaling are explored, and PERK inhibitor GSK2656157 is shown to enhance the anti-tumor effects of MPPα-PDT in HOS cells via regulation of autophagy by p21. Possible factors and potential molecular mechanisms are discussed, and the results may indicate a new therapeutic strategy against OS.

MATERIALS AND METHODS

Cell culture

HOS cells were purchased from ATCC (USA). Dulbecco's modified Eagle medium (Gibco, USA), supplemented with 10% fetal bovine serum (Wisent, Quebec, Canada) and 100 μg/mL pen/strep (Beyotime Biotech, Shanghai, China) was used to culture HOS cells at 37°C with 5% CO_2.

In vitro MPPα-PDT treatment

Conditions and procedures were identical to those described in our previous studies [10, 11, 19]. HOS cells were randomly grouped as follows: control (drug and LED-free); MPPα (incubation with 0.15 μM MPPα, Sigma-Aldrich); LED (drug free); and MPPα-PDT (incubation with 0.15 μM MPPα). Cells in all groups were incubated for 20 h without lighting. The cells of the MPPα-PDT and LED groups were then incubated with drug-free medium and subjected to light from LED equipment (Chongqing Jingyu Laser Technology Co., Ltd., Chongqing, China) at 630 nm wavelength and light energy density of 4.8 J/cm2 for 120 s.

Hoechst staining

HOS cells were subjected to different treatments. Twelve hours post-treatment, they were rinsed with 1× phosphate-buffered saline (PBS, Beyotime Biotech) and fixed with 4% paraformaldehyde. Nuclei were visualized using 10 μg/mL Hoechst 33258 (Beyotime Biotech). The cells were then imaged by fluorescence microscopy (Nikon, Tokyo, Japan).

Apoptotic assay

After HOS cells had been exposed to different treatments for 12 h, their apoptosis rates were detected by flow cytometry after Annexin V-FITC/propidium iodide (PI) (Beyotime Biotech) double staining.

Cell cycle analysis

HOS cells were placed in six-well plates at a density of 5×10^6 cells/well and subjected to different treatments for 12 h. The adherent cells and those in the basic medium and PBS were all collected, centrifuged at

1000 rpm for 5 min, and fixed overnight in PBS containing 75% ethanol at 4°C. The ethanol was removed by washing with PBS, and the intracellular RNA was digested by RNase A (200 μg/mL) for 30 min at 37°C. The cells were then stained with PI dye (50 μg/mL) for 30 min at 4°C without light before detection of the cell cycle distribution by flow cytometry.

Fluo-4 AM staining

After undergoing different treatments for 12 h, HOS cells were incubated with Fluo-4 AM (Beyotime Biotech) at a concentration of 2 μM at 37°C for 30 min while protected from light. They were then harvested and centrifuged, and the fluorescence intensity of cytosolic-free calcium was examined by flow cytometry.

Electron microscopy

After treatment with different interventions on 24-well culture plates, HOS cells were harvested and fixed with osmic acid and glutaraldehyde. Sections were prepared as previously reported before analysis by transmission electron microscopy (TEM).

Immunofluorescence

Following treatment, processed HOS cells were stabilized using 4% paraformaldehyde for a duration of 20 min, made permeable with 0.1% Triton-X 100 for 5 min, and then blocked using 3% bovine serum albumin (BSA) and 0.08% glycine for a period of 50 min. Samples were incubated with polyclonal rabbit anti-phospho-PERK antibody (bs-3330R, Bioss, USA) at 1:150 overnight at 4°C and then with FITC-conjugated goat anti-rabbit secondary antibody (bs-0295G-FITC, Bioss) at 1:200 for 1 h. For sections, paraffin-embedded slides were prepared as described in section 2.14 (Histology). Sections were deparaffinized, hydrated and subjected to antigen retrieval as described previously. For immunofluorescence (IF) examination of tissues, sections were also permeabilized and blocked before incubation with anti-phospho-PERK primary antibody and goat anti-rabbit Fluor 594 secondary antibody (bs-0295G-AF594, Bioss). Then, nuclei were visualized with DAPI (Beyotime Biotech) staining, and samples were imaged by fluorescence microscopy. Fluorescence intensity was analyzed using ImageJ 1.52.

RT-qPCR

RNA of treated HOS cells was isolated using RNAiso Plus (Cat. No. 9108, Takara, Japan), and mRNA (1 mg) was reverse transcribed using an RT-PCR assay kit (Cat. No. 6110A, RR901A, Takara). The primers used in this study were as follows: human p21: F: 5′-GCCCGTGAGCGATGGAACTTC-3′, R: 5′-CCTGCCTCCTCCCAACTCATCC-3′; human ATF4: F: 5′-GTCTGCCCGTCCCAAACCTTAC-3′, R: 5′-TCCTGCTCCGCCCTCTTCTTC-3′; human GAPDH: F: 5′-AGGTCGGTGTGAACGGATTTG-3′, R: 5′-TGTAGACCATGTAGTTGAGGTCA-3′. GAPDH was used as a control. SYBR green/fluorescein qPCR Master Mix (Cat. No. RR820A, Takara) was used for the PCR reaction. For RT-PCR amplification, 40 cycles were carried out at 95°C for 30 s, 95°C for 5 s, and 60°C for 30 s, using a CFX96 real-time PCR system (Bio-Rad, USA). The ΔΔCt method was used to evaluate the relative expression levels of genes.

Chromatin immunoprecipitation (ChIP)

ChIP assays were performed following the SimpleChIP® protocol (Agarose Beads) (https://www.cellsignal.com/contents/resources-protocols/simplechip-sup-sup-chromatin-immunoprecipitation-protocol-(agarose-beads)/chip-agarose) by Cell Signal Technology (USA). Purified DNA was analyzed by RT-qPCR. Protein–DNA complexes were cross-linked with formaldehyde and then subjected to nuclei preparation and chromatin digestion by sonication. Anti-ATF4 antibody (11815) was used at 1:200 for ChIP with normal rabbit IgG (3900) as negative control. ChIP-grade protein G agarose beads (9007) were used to harvest DNA–protein complexes. RNase A (No 7013) and proteinase K (10012) were used to treat the precipitates. All reagents used in the ChIP assays were purchased from Cell Signaling Technology. The primer sequences used were as follows [20]: 9-1 (p21 int1): F: 5′-CCAAGAGCGCTGTCAAGAAGA-3′, R: 5′-AGGAATTCAGCTGCTGGAGG-3′. The PCR were conditions as described above.

Short interfering RNA (siRNA) transfection

siRNAs against ATF4 and p21 and a negative control (siRNA-NC) were purchased from Hanbio Biotechnology Co., Ltd. (Shanghai, China). Lipo8000 (Beyotime, Biotech) was used for siRNA transfection following the manufacturer's instructions. Transfected HOS cells were incubated for 24 h for further examination. RT-qPCR and western blotting were used to determine relative mRNA and protein levels before and after transfection. The following siRNAs were used [21]: human p21 siRNA: 5′-GAUGGAACUUCGACUUUGU-3′; human ATF4 siRNA: 5′-GCCUAGGUCUCUUAGAUGA-3′; human p21 over-expression: LV-h-CDKN1A-E/B-F: CTAGAGGATCTATTTCCGGTGAATTCGCCACCATGTCAGAACCGGCTGGG. LV-h-CDKN1A-E/B-R CACTTAAGCTTGGTACCGAGGATCCGGGCTTCCTCTTGGAGAAGATCAG.

Western blotting

The western blot procedure was as outlined in our previous research. In short, both HOS cells and tumors were lysed using chilled RIPA buffer (Beyotime, Biotech), combined with a phosphatase and protease inhibitor cocktail (Bioss). After separation by 10% or 12% sodium dodecyl sulfate polyacrylamide gel electrophoresis, the proteins were transferred onto polyvinylidene fluoride membranes (Beyotime Biotech), which were then blocked with 5% non-fat milk for 2 h. The membranes were incubated with the following primary antibodies for a duration exceeding 12 h at a temperature of 4°C: anti-PERK (5683), anti-CHOP (2895), anti-BiP (3177), anti-ATF4 (11815), anti-LC3B (3868), anti-SQSTM1/p62 (88588), anti-Atg5 (12994) anti-cleaved caspase-3 (9664), anti-cleaved PARP (5625), anti-p21 (2947) all at 1:1000, and anti-phospho-eIF2α (3398) at 1:800, all from Cell Signaling Technology. Anti-β-actin (bs-0061R) at 1:5000, anti-phospho-PERK (bs-3330R) at 1:800, and anti-GAPDH (bs-0755R) at 1:5000 from Bioss were also used. Then, the membranes were further incubated with the corresponding HRP-labeled secondary antibodies. Detection was carried out using BiossECL Plus WB Substrate (Bioss), and band intensities were analyzed using Image Lab software.

Xenograft model, MPPα-PDT therapy, and GSK2656157 treatment *in vivo*

The animal studies received approval from the relevant ethical board. Male nude mice, 5 weeks old, were procured from the Chongqing Medical University's Experimental Animal Center (certificate: SCXK (Yu) 2012–0001). These animals were housed in an environment with regulated temperature and humidity, following a 12-h light/dark cycle, and were granted unrestricted access to food and water. Xenograft model generation and MPPα-PDT treatment were done as described previously [9]. Briefly, nude mice were anesthetized and injected subcutaneously in the back with 100 μL PBS containing 1×10^6 HOS cells. When tumors reached 8 ± 1 mm in diameter, animals were split into six groups (three mice in each group): the control, MPPα, LED, GSK2656157 (S7033, Selleck, USA), MPPα-PDT, and MPPα-PDT+GSK2656157 groups. MPPα was injected into the tail vein at 15 mg/kg, and the animals were held in a dark room for 18 h to allow biodistribution of MPPα into the tumor. They were then exposed to 630 nm light at 120 J/cm2, for 20 min every other day, for 10 days. GSK2656157 was prepared in a solution composed of 0.5% hydroxypropyl methyl cellulose and 0.1% Tween-80 in water with a pH of 6.75 and orally administered at 50 mg/kg twice daily [22]. Tumor volume was monitored every 4 days for 30 days after treatment and calculated as follows: tumor volume = (length × width2)/2.

Histology

Fresh tissue was fixed with 4% formaldehyde for more than 24 h, dehydrated with an increasing alcohol concentration gradient, and embedded in paraffin. The wax block was sliced to a thickness of 1 mm. Slides were then incubated in hematoxylin and eosin.

Immunohistochemistry (IHC)

Slices were dried in an oven at 60°C and dewaxed by soaking in different concentrations of xylene and ethanol. The sections were placed in an antigen repair solution prepared in advance. Then, 3% H_2O_2 was added to remove endogenous peroxidase, and 1% BSA was added for blocking. Primary antibody was added to the tissue, with incubation overnight at 4°C, followed by further incubation with secondary antibody at 37°C. Hematoxylin was used to stain the nuclei. Finally, the sections were observed and recorded under a microscope at a 200X magnification. IHC quantification was done using IHC Profiler according to the following levels: 4, high positive; 3, positive; 2, low positive; 1, negative.

TUNEL assay

Slices were soaked in xylene and different concentrations of ethanol (twice with 100% for 3 min, then with 85% for 3 min and 75% for 3 min) before treatment with proteinase K (0.5%) for 25 min at 37°C and Triton-X-100 for 20 min at room temperature. A TUNEL assay kit (Cat. No. 11684817910, Roche Diagnostics, USA) was used according to the manufacturer's instructions. Briefly, the TUNEL reaction mixture (TdT + dUTP mixed at a 1:9 ratio) was prepared according to the instructions, added to sections, and allowed to react for 2 h at 37°C. Nuclei were stained with DAPI at room temperature for 10 min. Apoptotic cells were examined under a fluorescence microscope.

GFP-LC3 transfection

HOS cells, at a quantity of 1×10^5 per well, were placed in a confocal dish. Following a 24-h culture period post-treatment, adenovirus GFP-LC3 (Hanbio, Shanghai, China) was introduced, and the cells were left for another 24 h. Visual data were acquired using laser confocal microscopy (TCS-SP5, Leica, Germany). The count of green fluorescent specks was considered to indicate the extent of autophagy.

Mitochondrial membrane potential assay

A JC-1 staining kit (Beyotime Biotech, China) was used to evaluate the mitochondrial membrane potential (ΔΨm) of treated HOS cells. Post-treatment, a staining buffer was introduced and left for 20 min at a temperature of 37°C. The staining of HOS cells was observed and assessed through fluorescence microscopy and flow cytometry.

Data analysis and statistics

Data are presented as the mean ± standard deviation. Data measurements were analyzed using Student's *t*-test or analysis of variance in GraphPad Prism 7. Every experiment was conducted a minimum of three times. A value of $p < 0.05$ was deemed to indicate statistical significance.

Data availability

The datasets used or analyzed during the current study are available from the corresponding author on reasonable request.

RESULTS

MPPα-PDT induces apoptosis and cycle arrest

To explore the anti-tumor mechanism of MPPα-PDT, we examined a series of apoptotic indicators. HOECHST staining revealed apoptotic morphological changes, including nuclear fragmentation and chromatin condensation, following 12 h MPPα-PDT treatment (Figure 1A). No marked changes were observed in the control, MPPα and LED groups. Concurrently, we investigated apoptosis-related proteins, including cleaved caspase-3 and cleaved PARP, using western blot analysis. Levels of cleaved caspase-3 and cleaved PARP both increased in response to MPPα-PDT treatment at 3, 6, and 12 h ($P \leq 0.01$, Figure 1B, 1C). Further, we used flow cytometry to evaluate the influence of MPPα-PDT on the cell cycle and apoptosis ($P \leq 0.01$, Figure 1D–1F). Following MPPα-PDT treatment, a significant increase was observed in the proportion of HOS cells arrested in the G0/G1 phase, accompanied by notable reductions in the percentages of cells residing in the S and G2/M phases ($P \leq 0.05$, Figure 1E–1G). There were no discernible variations in cell cycle distribution in the remaining three groups ($P \geq 0.05$, Figure 1E–1G). The G0/G1 phase denotes the initial stage of cellular division wherein cells undergo growth and prepare for entry into the S phase of DNA replication. By impeding progression through the cell cycle during this specific phase, a multitude of effects can be elicited, including inhibition of cellular proliferation, heightened treatment sensitivity, induction of apoptosis, suppression of DNA replication, and reduction in relapse. These findings suggest that MPPα-PDT can trigger G0/G1 cell cycle arrest and apoptosis in HOS cells. No noticeable differences in the distribution of cell cycle phases were found among the other three groups ($P \geq 0.05$, Figure 1E–1G). This evidence points towards an ability of MPPα-PDT ability to induce G0/G1 cycle arrest and apoptosis in HOS [7, 8, 11].

MPPα-PDT triggers ER stress and PERK-eIF2α-ATF4 signaling pathway activation

PDT can produce large amounts of ROS, which may disrupt ER REDOX regulation and homeostasis, leading to ERS and an increase in misfolded/unfolded proteins. Therefore, we preliminarily investigated whether ERS is involved in the potential mechanism of MPP-α-PDT anti-tumor by transmission electron microscopy (TEM). As we observed, the ER of HOS cells showed significant morphological damage after MPPα-PDT treatment, indicating the occurrence of ERS (Figure 2A). The ER is a dynamic organelle involved in various cellular functions, including the regulation of lipid metabolism, calcium storage, and protein balance. During stress, calcium ions are released from the ER into the cytoplasm, initiating a cascade of cell signaling pathways and physiological responses. Therefore, it is crucial to detect calcium ion leakage during ER stress to gain insights into the signal transduction network and physiological response within the cell. As shown in Figure 2B, relative to the other three groups, intracellular Ca^{2+} concentration ($(Ca^{2+})i$) was much higher in the MPPα-PDT treatment group. Western blotting was used to determine whether PERK-eIF2α-ATF4 signaling was activated by MPPα-PDT. The data revealed a significant increase in PERK-eIF2α-ATF4 signaling-related proteins, including p-PERK, BIP, p-eIF2α, ATF4, and CHOP, following MPPα-PDT treatment ($P \leq 0.05$, Figure 2C, 2D). These findings indicate that MPPα-PDT induces characteristic manifestations of ER stress such as disrupted ER morphology, elevated intracellular calcium concentration ($(Ca^{2+})i$), and activated PERK-eIF2α-ATF4 signaling.

Autophagy can be triggered by MPPα-PDT

Autophagy is a highly conserved decomposition process regulated by genes. Generally, it is a regulatory mechanism by which cells resist adverse stress or external damage. Thus, we tested whether autophagy was involved in the mechanism of MPPα-PDT. First, abundant autophagosomes in the MPPα-PDT group were observed through TEM analysis

(black arrows, Figure 3A). Moreover, western blot analysis revealed elevated LC3-II/LC3-I ratios and ATG5 levels, as well as significantly reduced p62 levels, in HOS cells after MPPα-PDT treatment ($P \leq 0.05$, Figure 3B–3D). Taken together, these results indicate that MPPα-PDT can induce autophagy.

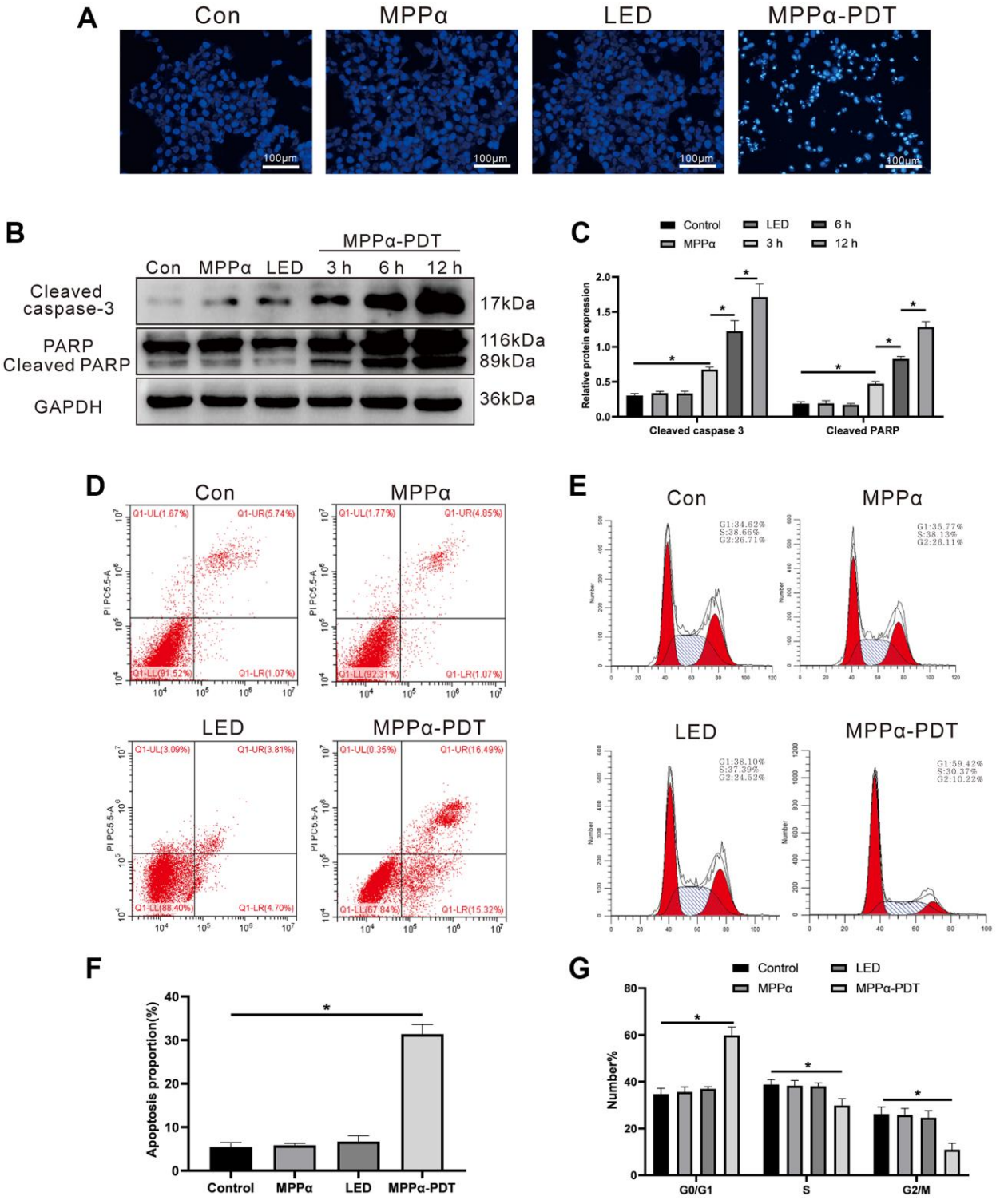

Figure 1. MPPα-PDT induces HOS cells cycle arrest and apoptosis. (**A**) HOS cells nuclei were examined for apoptotic morphological changes under a fluorescence microscope (magnification: ×200) after MPPα-PDT treatment for 12 h. (**B**, **C**) Cells were harvested after MPPα-PDT treatment for 3, 6, and 12 h and western blot used to evaluate cleaved caspase-3 and cleaved PARP levels. (**D**–**F**) Apoptosis was determined by flow cytometry. (**E**–**G**) Cell cycle distribution was analyzed using flow cytometry. $^{*}P < 0.05$ vs. control group. All data represent the mean ± SD of 3 independent experiments.

Blocking PERK can inhibit autophagy triggered by MPPα-PDT and augment the anti-tumor efficacy of MPPα-PDT in HOS cells

Having demonstrated that ER stress and autophagy could be induced by MPPα-PDT, we further explored this relationship. To achieve complete inhibition of the PERK pathway, we pretreated HOS cells with PERK inhibitor GSK2656157 (5 mM; Selleck Chemicals, Cat. No. S7033) for 2 h. Increased p-PERK fluorescence intensity was observed by IF after MPPα-PDT treatment ($P \leq 0.05$ Figure 4A, 4B). Western blot analysis showed that MPPα-PDT increased p-PERK and ATF4 levels and reduced PERK levels ($P \leq 0.01$, Figure 4C, 4D), demonstrating that the activation of PERK induced by MPPα-PDT could be reversed by GSK2656157. Moreover, the anti-tumor effect of MPPα-PDT was markedly strengthened after GSK2656157 treatment, as reflected by an increase in levels of apoptotic proteins. Changes in the expression of LC3-II/I and p62 indicated successful autophagy blocking after bafilomycin A1 pretreatment, with similar inhibitory effects observed

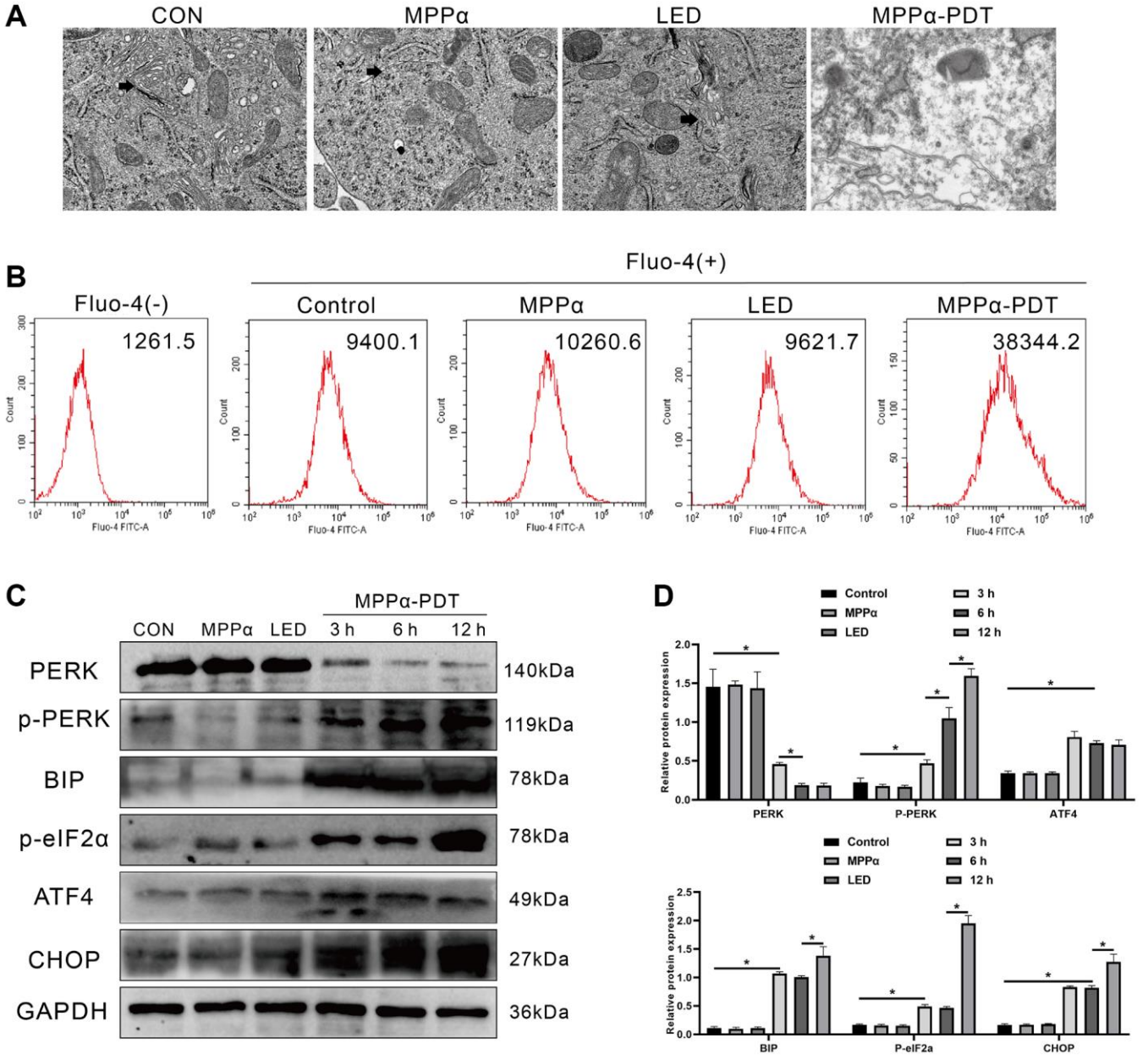

Figure 2. ER stress and PERK-eIF2α-ATF4 signaling pathway activation are induced by MPPα-PDT in HOS cells. (**A**) ER morphology was observed by TEM (magnification, ×20000). (**B**) Intracellular Ca^{2+} concentration was quantified by flow cytometry using Fluo-4-AM probe. (**C**, **D**) MPPα-PDT treated cells were harvested after 3, 6, and 12 h and PERK, p-PERK, BIP, p-eIF2α, ATF4, and CHOP, levels determined by western blot. Data are shown as mean ± SD of 3 independent experiments. $^{*}P < 0.05$ vs. control group.

for GSK2656157 ($P < 0.05$, Figure 4E–4G). These findings were supported by the flow cytometry results ($P \leq 0.05$ Figure 4H, 4I). In summary, our results indicate that PERK-eIF2α-ATF4 signaling blockade may suppress protective autophagy and other pro-survival mechanisms.

Targeting ATF4 increases the sensitivity of PDT by inhibiting autophagy

ATF4, a downstream effector of the PERK pathway, mediates the adaption of cells to harmful conditions such as ER stress, and modulates expression of various pro-survival factors including p21. We used western blotting to determine whether induction of p21 expression by MPPα-PDT requires ATF4. Anti-ATF4 siRNA significantly suppressed ATF4 expression and cell viability ($P \leq 0.01$, Figure 5A, 5B, Supplementary Figure 1). ATF4 and p21 levels were upregulated by MPPα-PDT, whereas ATF4 depletion suppressed p21 induction by MPPα-PDT. PERK signaling blockade by GSK2656157 pretreatment suppressed ATF4 and p21 induction by MPPα-PDT. Apoptosis proteins PARP and cleaved-caspase 3 were activated by GSK2656157 or siRNA-ATF4 under MPPα-PDT treatment ($P \leq 0.05$, Figure 5C, Supplementary Figure 2). Levels of apoptosis were detected by flow cytometry and JC-1 staining (Figure 5D, 5E). Autophagy was found to be activated by MPPα-PDT but inhibited by GSK2656157 or siRNA-ATF4, as indicated by the levels of autophagy proteins including LC3, P62, and Beclin 1, and of GFP-LC3 fluorescent particles (Figure 5F, 5G, Supplementary Figure 3). Thus, as the key effector of PERK pathway, ATF4 is a potential target that could be used to enhance the efficacy of MPPα-PDT.

The pro-survival effect of p21 is achieved by regulation of autophagy after MPPα-PDT

Cyclin-dependent kinase inhibitor (CDKI/P21) is the target gene encoded by ATF4, and promotes cell survival under ER stress. Past studies have shown that ATF4 binds in the first intron of p21 at +710 to +724 (GCGCTGAGGTCAGCG) to induce p21

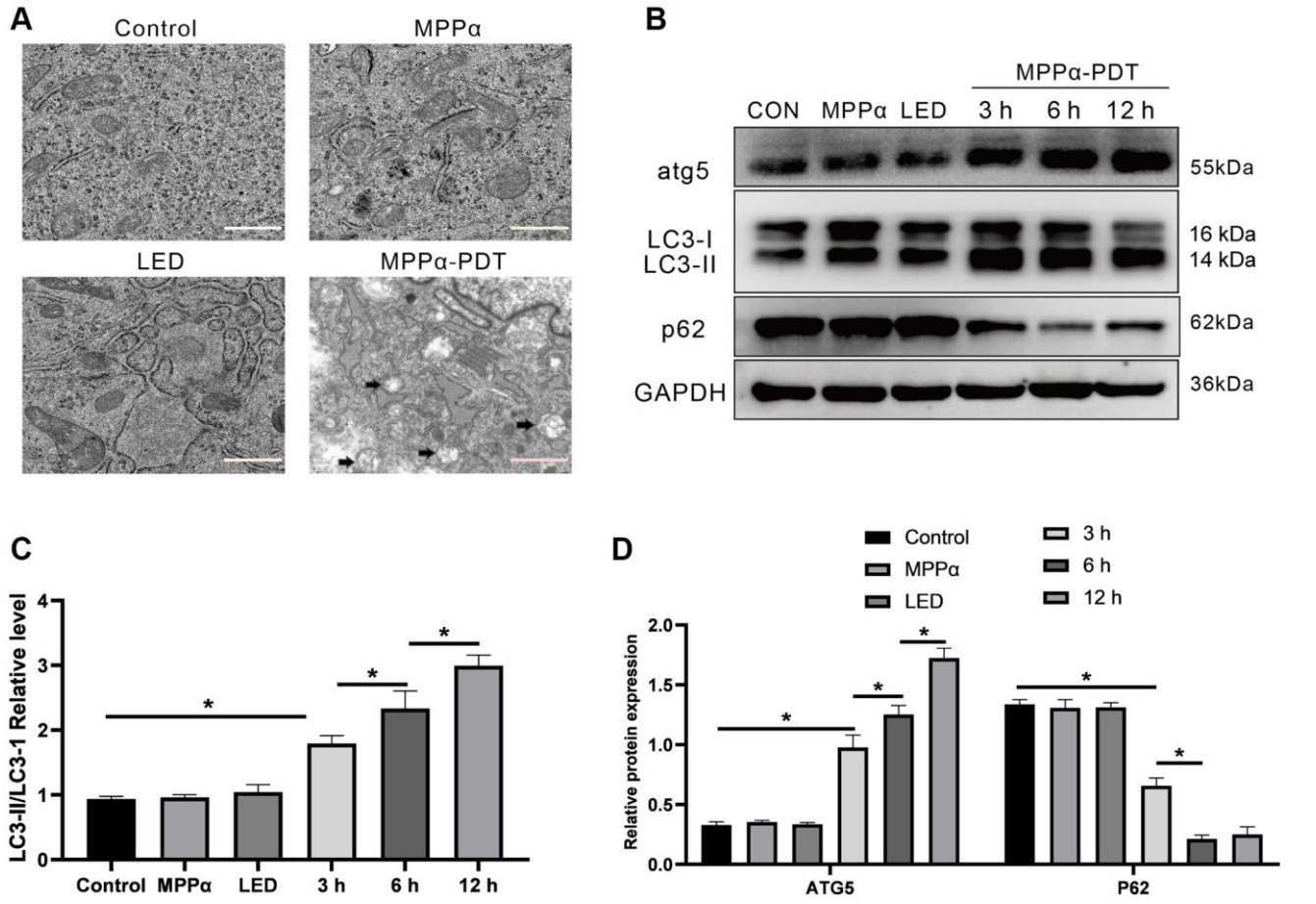

Figure 3. Autophagy can be triggered by MPPα-PDT. (**A**) Transmission electron microscopy (magnification, ×20000) was used to observe autophagosomes upon autophagy induction by MPPα-PDT after 12 h. (**B**–**D**) Cells were harvested 3, 6, and 12 h after MPPα-PDT treatment and protein ATG5, LC3-II/LC3-I, and p62 were determined by western blot. Data are shown as mean ± SD of 3 independent experiments. $^{*}P < 0.05$ vs. control group.

expression [20]. Here, ChIP analysis showed that ATF4 bound to the first intron of p21 after MPPα-PDT treatment (Figure 6A). Next, we sought to elucidate the role of p21 in PERK signaling activation. To this end, we used western blotting to determine the influence of p21 on the survival of HOS cells. Compared with the

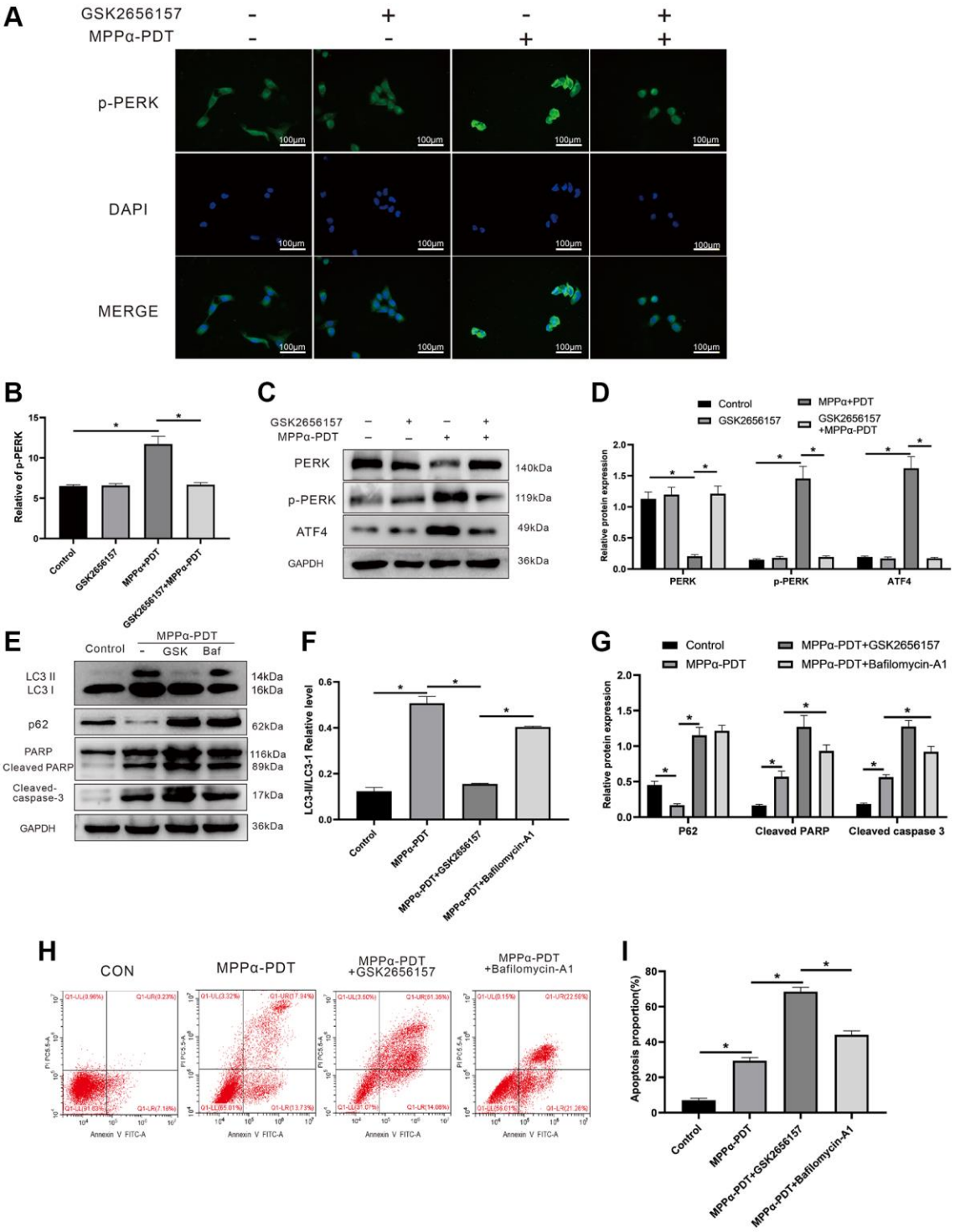

Figure 4. Inhibiting PERK may suppress autophagy induced by MPPα-PDT, and enhance the anti-tumor ability of MPPα-PDT in HOS cells. HOS cells in MPPα-PDT+GSK2656157 group were pretreated with 5 mM GSK2656157 for 1 h before MPPα-PDT treatment. HOS cells in MPPα-PDT + Bafilomycin A1 group were pretreated with 100 nM bafilomycin A1 for 2 h before MPPα-PDT treatment. (**A**, **B**) Immunofluorescence analysis of p-PERK levels (magnification: ×400). (**C**–**G**) After indicated treatments, cells were harvested and PERK, p-PERK, ATF4, LC3-II/LC3-I, p62, cleaved caspase-3, and cleaved PARP levels determined by western blot. (**H**, **I**) Apoptotic rate was examined by flow cytometry. Data are shown as mean ± SD of 3 independent experiments. $^{*}P < 0.05$.

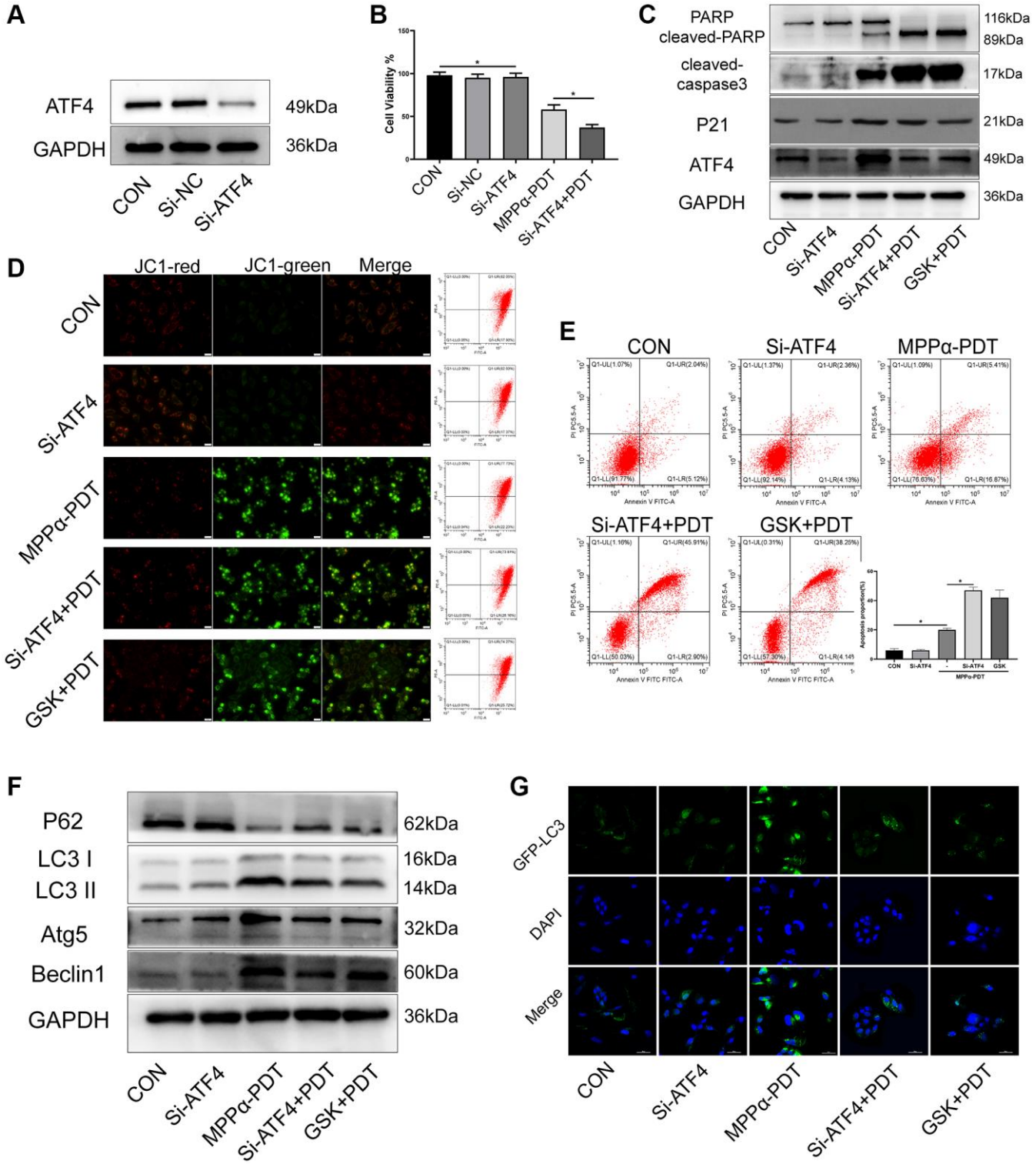

Figure 5. Targeting ATF4 increases the sensitivity of PDT by inhibiting autophagy. HOS cells in MPPα-PDT+GSK2656157 group were pretreated with 5 mM GSK2656157 for 1 h before MPPα-PDT treatment. HOS cells were transfected with siRNAs and then treated with MPPα-PDT. (**A**) Protein ATF4 or mRNA ATF4 was detected by western blot and represents the transfection efficiency. (**B**) Cell viabilities were detected by CCK-8 after treated with SiRNA-ATF4 (Si-ATF4), SiRNA-negative control (Si-NC), MPPα-PDT and group MPPα-PDT combined with Si-ATF4. (**C**) Following indicated treatments, cells were harvested and ATF4, p21, PARP and cleaved caspase-3 levels determined by western blot. (**D**, **E**) Apoptotic rate or JC-1 stain was examined by flow cytometry or fluorescence microscope (×200). (**F**) Following indicated treatments, cells were harvested and LC3, P62, Atg5 and Beclin1 levels were determined by western blot. (**G**) Adenovirus-GFP-LC3 was transfected into the HOS cells after treated, the LC3 fluorescent particles were observed by laser confocal microscope (×400). $^{*}P < 0.05$ vs. control group, data are shown as mean ± SD of 3 independent experiments.

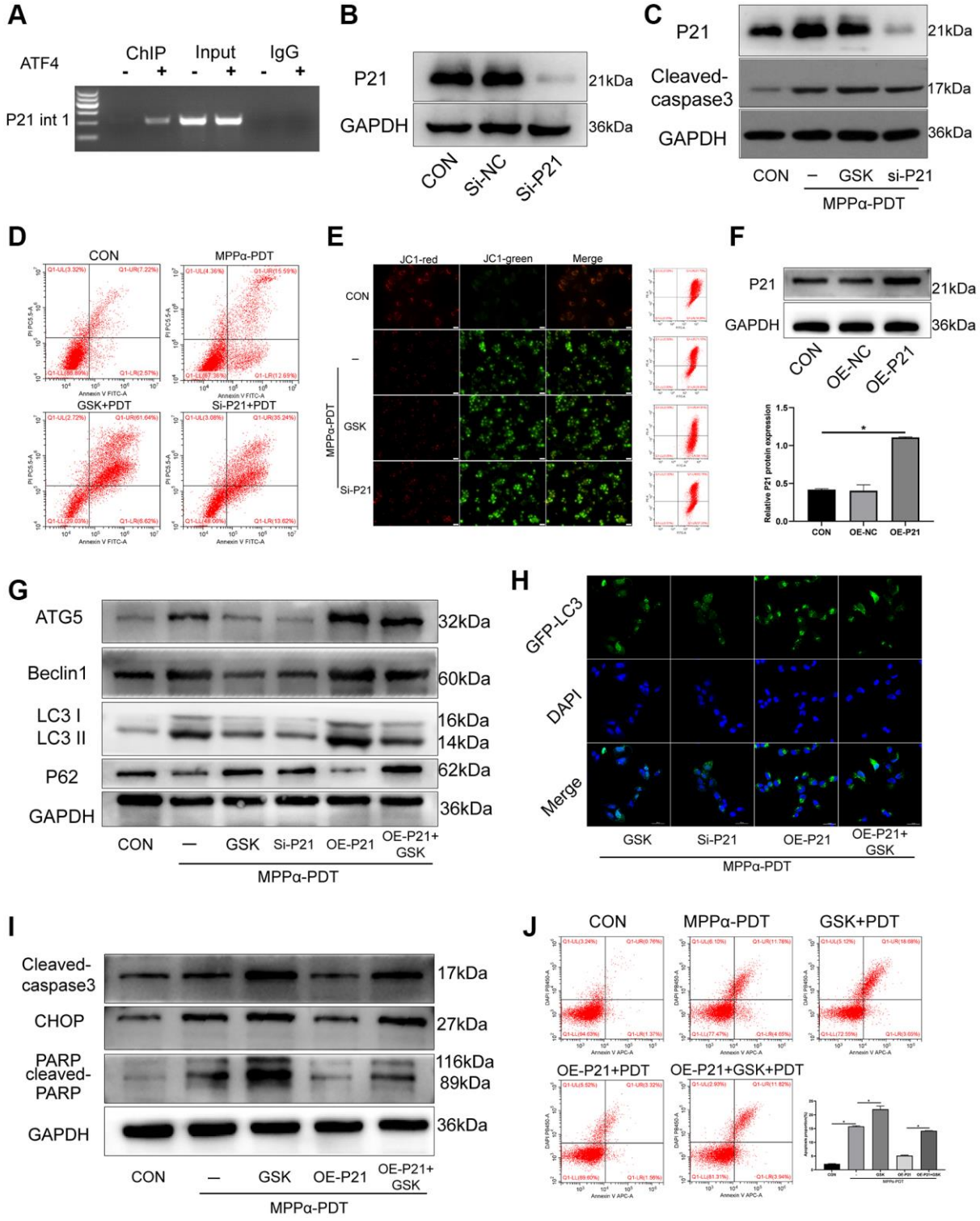

Figure 6. The pro-survival effect of P21 is achieved by regulating autophagy after MPPα-PDT. (**A**) ChIP analysis was used to detect ATF4 binding to the first intron of p21. HOS cells were transfected with siRNAs and then treated with MPPα-PDT. (**B**) Protein P21 were detected by western blot to represent the transfection efficiency. (**C**) Following indicated treatments, cells were harvested and P21 and cleaved caspase-3 levels were determined by western blot. (**D**, **E**) Apoptotic rate or JC-1 stain were examined by flow cytometry or fluorescence microscope (×200). (**F**) Protein P21 was detected by western blot after transfected by lentivirus-overexpress P21. (**G**) Following indicated treatments, cells were harvested and LC3, P62, Atg5 and Beclin1 levels were determined by western blot. (**H**) Adenovirus-GFP-LC3 was transfected into the HOS cells after treated, the LC3 fluorescent particles were observed by laser confocal microscope (×400). (**I**) Protein CHOP, cleaved-caspase3 were detected by western blot. (**J**) Apoptotic rate was examined by flow cytometry. $^{*}P < 0.05$ vs. control group, data are shown as mean ± SD of 3 independent experiments.

MPPα-PDT group, cells in the p21-silencing group had increased cleaved caspase-3 levels. Similarly, PERK inhibition with GSK2656157 pretreatment reduced p21 levels but upregulated cleaved capase-3, relative to levels in the MPPα-PDT group ($P \leq 0.05$, Figure 6B, 6C, Supplementary Figures 4 and 5). Apoptosis analysis by flow cytometry revealed that p21 depletion enhanced the cytotoxicity of MPPα-PDT ($P \leq 0.05$, Figure 6D, 6E). These data indicate that induction of p21 expression by ATF4 may promote survival of HOS cells. PERK-eIF2α-ATF4 signaling inhibition enhanced MPPα-PDT cytotoxicity by reducing p21 expression. Next, p21 was overexpressed using a lentivirus vector, and the transfection efficiency was detected by western blotting ($P \leq 0.05$, Figure 6F). Autophagy was found to be activated by p21 overexpression after treatment with MPPα-PDT ($P \leq 0.05$, Figure 6G, 6H, Supplementary Figure 6). Moreover, apoptosis proteins including PARP, CHOP, and cleaved-caspase 3 were inhibited by p21 overexpression after MPPα-PDT treatment ($P \leq 0.05$, Figure 6I, 6J, Supplementary Figure 7). Briefly, these results indicate that the pro-survival effect of p21 is achieved by regulation of autophagy after MPPα-PDT treatment.

GSK2656157 enhances anti-tumor activity of MPPα-PDT by inhibiting PERK pathway *in vivo*

Next, we examined whether GSK26556157 enhanced MPPα-PDT efficacy against HOS *in vivo* by evaluating tumorigenicity in a xenograft mouse tumor model following various treatments. Tumor volume was monitored every 4 days, and tumor size growth curves were drawn ($P \leq 0.05$, Figure 7A–7C). Treatment with MPPα-PDT decreased the proliferation of tumors compared with the control group, and MPPα-PDT in combination with GSK2656157 enhanced anti-tumor effects relative to MPPα-PDT alone. Hematoxylin and eosin staining analysis of tumor tissues revealed large necrosis areas following MPPα-PDT treatment, which were enhanced by combination treatment with GSK2656157 ($P \leq 0.05$; Figure 7D). TUNEL staining revealed elevated apoptosis in the MPPα-PDT and MPPα-PDT+GSK2656157 treatment groups, with a greater increase in the latter ($P \leq 0.05$, Figure 7D, 7E). To establish whether GSK2656157 treatment enhances the cytotoxicity of MPPα-PDT, we used western blotting to assess cleaved caspase-3 expression. The results showed that cleaved caspase-3 expression levels were elevated by MPPα-PDT and were higher still in the MPPα-PDT+GSK2656157 group ($P \leq 0.05$, Figure 7F, 7G).

p-PERK *in vivo* levels following treatments

p-PERK is both a sign of PERK signaling activation and a target of GSK2656157 inhibition. IHC analysis revealed lower positive p-PERK levels in the control, MPPα, and LED groups compared with those in the MPPα-PDT group. On the contrary, p-PERK levels were markedly reduced by GSK2656157 alone and by MPPα-PDT+GSK2656157 ($P \leq 0.01$, Figure 8A, 8B). Analysis of p-PERK levels by IF gave similar results to those obtained with IHC. MPPα-PDT significantly elevated p-PERK expression, whereas GSK2656157 reduced it alone or in combination with MPPα-PDT ($P \leq 0.01$, Figure 8C, 8D). Western blotting results showed that relative to controls, p-PERK levels were elevated by MPPα-PDT but suppressed by GSK2656157 alone or in combination with MPPα-PDT ($P \leq 0.01$, Figure 8E, 8F). These results indicate that MPPα-PDT has anti-tumor effects *in vivo*, which are enhanced by PERK inhibition with GSK2656157.

DISCUSSION

Among primary bone cancers, osteosarcoma is the most common, with a bimodal age distribution of onset, with the first peak occurring in patients aged 10–14 years and the second peak occurring in patients over 65 years, with about 25% of cases occurring in adults aged 20–59 years [23]. However, the underlying tumor biology of osteosarcoma in children and adults is significantly heterogeneous, including: chromosome instability [24], abnormal mitotic signaling pathways and cell cycle checkpoints [25], telomere dysregulation [26], and miRNA expression [27] et al. Compared to pediatric osteosarcomas, adult osteosarcomas are more likely to be secondary osteosarcomas associated with prior radiation therapy or, in some cases, Paget's disease (a disorder of bone metabolism characterized by overactivity of bone cells and the formation of bone matrix by osteoblasts in a faster and disordered manner, producing their characteristic "Mosaic" pattern [23]). Radiation exposure is another cause of secondary osteosarcoma in adults, typically occurring many years after the exposure. Osteosarcoma is also the most common bone tumor caused by radiation, accounting for 50–60% of cases [28]. Secondary osteosarcoma is associated with increased morbidity and mortality compared to primary bone tumors. Therefore, secondary osteosarcoma may result in poor overall prognosis estimates for adult osteosarcoma. The killing mechanism of PDT involves the activation of photosensitizers to generate photochemical reactions via external light of a specific wavelength. This causes production of abundant cytotoxic ROS, resulting in oxidative damage to tumor cells [29]. MPPα, a chemical substance extracted from chlorophyll with low toxic side-effects, is a second-generation photosensitizer. MPPα-PDT has been proven to have high-efficiency killing effects in various tumors [30, 31]. Similar to previous studies [6–8, 10], we observed apoptosis in HOS cells after

MPPα-PDT, as reflected by fragmented nuclei or increased levels of apoptotic proteins.

Owing to early lung metastasis and chemotherapy resistance, OS has a poor prognosis. To escape death, tumor cells deploy various signaling pathways to relieve cellular stress [32, 33]. Recent studies indicate that ER stress in response to anti-tumor therapy may disrupt ER function, thereby affecting protein synthesis, disturbing intracellular Ca^{2+} homeostasis, and contributing to

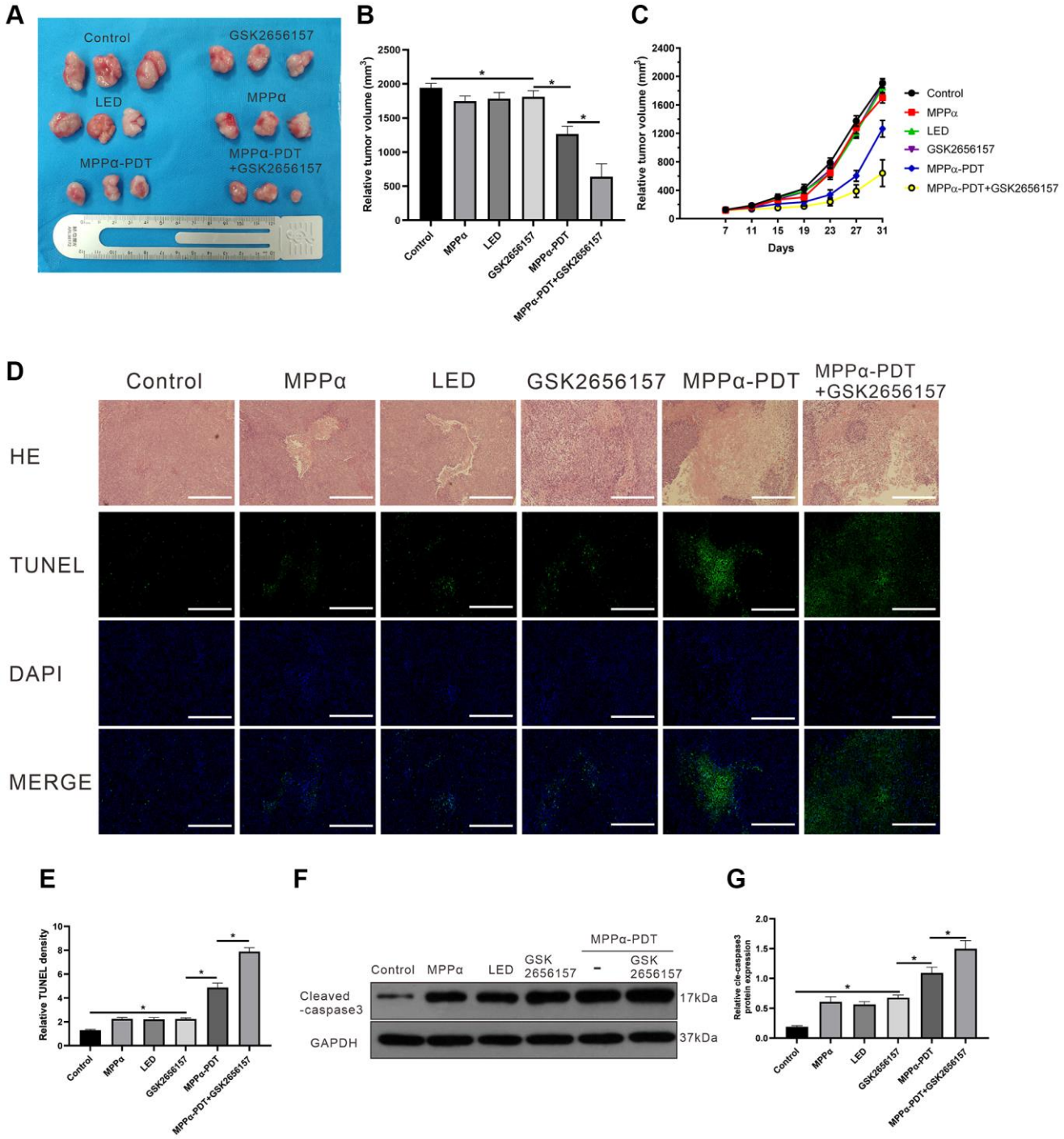

Figure 7. GSK2656157 enhances the antitumor activity of MPPα-PDT by inhibiting PERK pathway *in vivo*. HOS tumor-bearing mice were treated with MPPα (15 mg/kg), LED (120 J/mm2), GSK2656157 (30 mg/kg) and MPPα-PDT (LED following MPPα, as described in Materials and Methods). (**A**, **B**) After 31 days, tumors were collected. Tumor volume was determined as described in methods. (**C**) Tumor volume change curves. (**D**, **E**) After treatments, tumor necrosis and apoptosis were analyzed by H&E and TUNEL analysis, respectively (magnification, ×100). (**F**, **G**) After treatments, tumors apoptosis was assessed by cleaved caspase-3 western blot analysis. Data are shown as mean ± SD of 3 independent experiments. $^{*}P < 0.05$.

therapy resistance [34]. This may rely on the regulation of UPR signaling pathways (PERK, IRE1α, and ATF6). During ER stress, PERK can be released from GRP78, resulting in PERK kinase dimerization and autophosphorylation. In turn, this may lead to eIF2α phosphorylation, which may inhibit protein synthesis and CHOP/caspase-12 activation [19]. PERK signaling may be activated by various anti-tumor strategies to enhance survival of tumor cells. Ang Zhao et al. [35] showed that inhibition of OS cell proliferation by β-elemonic acid was accompanied by significant PERK signaling activation. Similarly, we found that PERK signaling could be also activated by MPPα-PDT, as reflected by an increase in expression of PERK-related proteins and concomitant ER stress events. Here, we sought to establish whether MPPα-PDT-induced PERK signaling is pro-death or pro-survival in HOS cells. We found that the PERK pathway could protect HOS cells

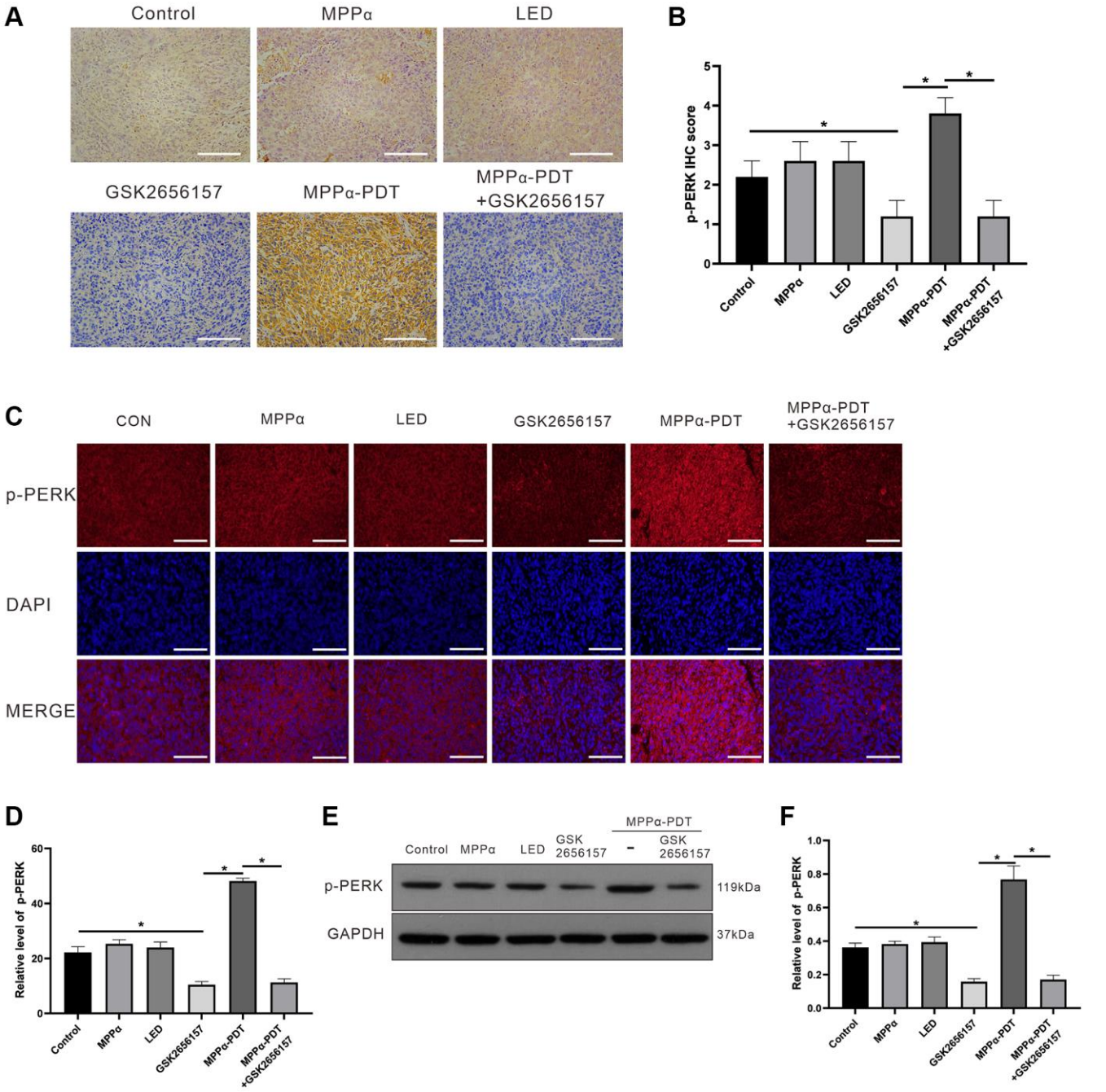

Figure 8. p-PERK *in vivo* levels upon indicated treatments. (**A**, **B**) IHC analysis of p-PERK levels in tumor sections (magnification, ×200). (**C**, **D**). Fluorescence analysis of p-PERK levels in tumor sections (magnification, ×400). (**E**, **F**) Following indicated treatments, tumor tissues were analyzed by western blot for p-PERK levels. Data are shown as mean ± SD of 3 independent experiments. [a]$P < 0.01$ vs. control group; [b]$P < 0.01$ vs. MPPα-PDT group.

from the cytotoxic effects of MPPα-PDT and that its inhibition could overcome the survival-promoting effects, enhancing the sensitivity of HOS cells to MPPα-PDT. Consistent with previous research, their findings demonstrate that disabling PERK signaling hinders the clonogenic and growth abilities of CML cells and amplifies apoptosis triggered by imatinib [34].

Autophagy is a major regulator of cellular metabolism, growth, and nutrient recycling and is required for tumor survival. Autophagy flux correlates with metabolic or therapeutic challenges. Previously, we showed that MPPα-PDT induced autophagy in MG63 cells, a HOS cell line [7]. Similarly, autophagic vacuoles were observed in HOS cells after MPPα-PDT treatment, and autophagic flux analysis revealed elevated expression of autophagy-related proteins after MPPα-PDT. Taken together, these data suggest that MPPα-PDT enhances autophagosome formation and autophagy in HOS cells. Autophagy is mainly involved in cellular survival under stress conditions. However, some studies have linked it to cell death paradoxically. To determine the role of autophagy during the MPPα-PDT treatment, we used an inhibitor, bafilomycin A1, to suppress cellular autophagy. Apoptosis was enhanced markedly by bafilomycin A1 pretreatment combined with MPPα-PDT, as reflected by the results of our analysis of proapoptotic factors and flow cytometry. PERK-eIF2α-ATF4 signaling shares some underlying molecular mechanisms on inducing autophagy. PERK-eIF2α-ATF4 signaling also comprises a unique molecular network in autophagy regulation upstream of mTORC1 [36, 37]. To determine whether autophagy could be mediated by PERK-eIF2α-ATF4 signaling, we inhibited PERK autophosphorylation using inhibitor GSK2656157. Reduced expression of PERK downstream factors (p-PERK and ATF4) was observed, resulting in autophagic flux attenuation in HOS cells. Given the protective role of autophagy in HOS cells after MPPα-PDT, we hypothesized that pro-

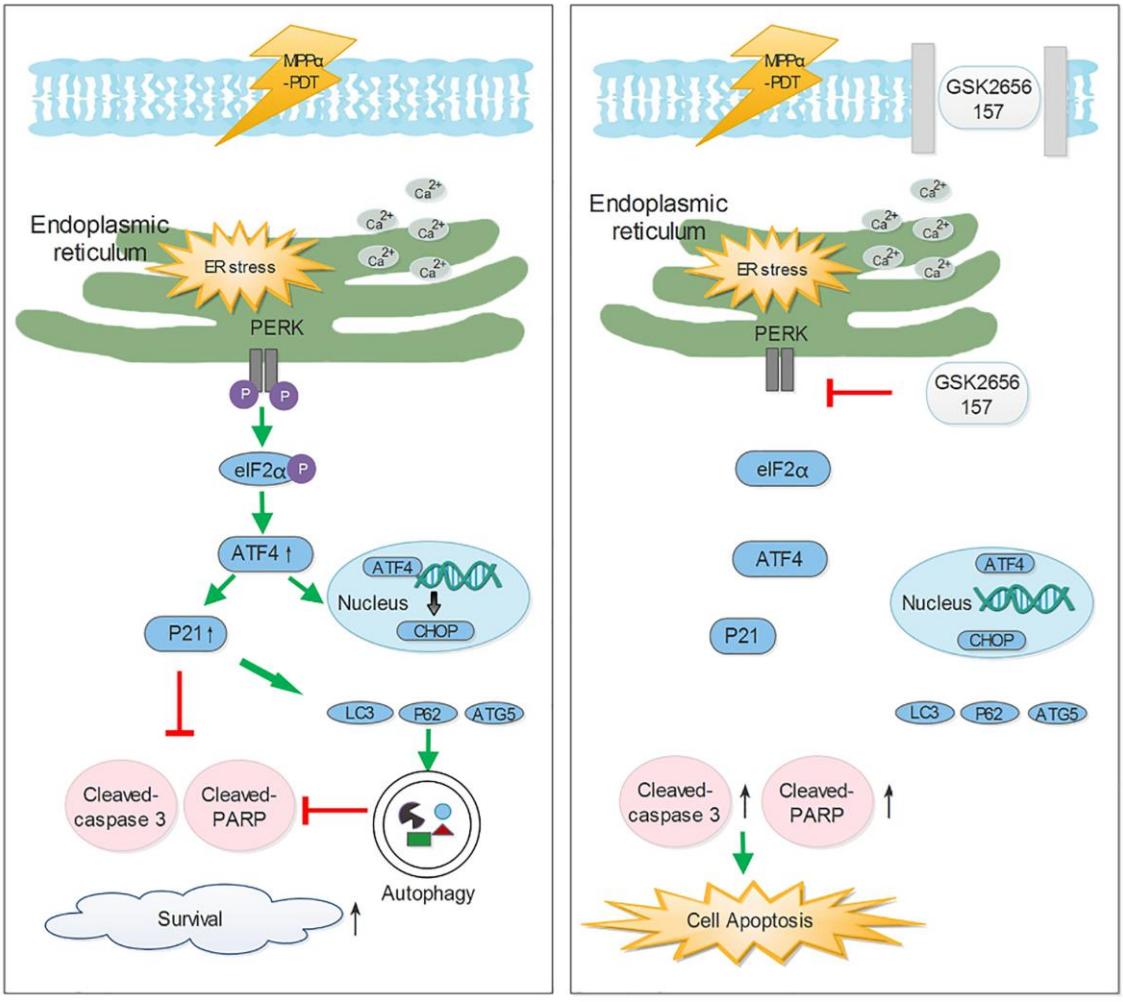

Figure 9. The potential mechanisms of inhibiting Perk-ATF4-P21 pathway to enhance the efficacy of MPPα-PDT. Antitumor ability of Mppα-PDT is improved by inhibiting PERK signaling, which is achieved by P21 regulating autophagy.

survival autophagy might be mediated by PERK-eIF2α-ATF4 signaling, which would be suppressed by PERK inhibitor GSK2656157. Our data show that apoptosis levels were much higher when MPPα-PDT was combined with GSK2656157 relative to MPPα-PDT alone or MPPα-PDT + bafilomycin A1, there were also higher expression levels of cleaved caspase-3 and cleaved PARP. Ji et al. [38] found that PERK depletion could suppress protective autophagy while enhancing stress sensitivity, potentially leading to apoptosis. These results indicate that PERK inhibition may suppress the protective effects of other mechanisms, as well as autophagy mediated by PERK signaling.

Another important theme that emerged from the data was that other protective mechanisms induced by PERK signaling may contribute to survival of HOS cells. ATF4 has a dual function in life–death decisions during treatment. Long-term, intensive stress may turn ATF4 into a pro-apoptotic factor that activates caspase-12-dependent, ER-stress-mediated apoptosis and elevated CHOP levels. On the contrary, ATF4 contributes to stress relief and survival through coping cytoprotective genes [39]. In the present work, we found that apoptosis proteins were activated by GSK2656157 or siRNA-ATF4 under treatment with MPPα-PDT. Apoptosis levels were detected by flow cytometry or JC-1 staining. As a key molecule in the PERK pathway that mediates autophagy, ATF4 can induce the formation of an ATG12-ATG5-ATG16 complex, which is associated with ATG8 and is involved in the formation of auto-phagosomes. Simultaneously, ATF4 activation induces increased downstream CHOP expression and inhibits the expression of the mTORC1 pathway, thereby enhancing autophagy activity [40]. We also found that autophagy was activated by MPPα-PDT but inhibited by GSK2656157 or siRNA-ATF4. Thus, as the key effector of the PERK pathway, ATF4 is a potential target that could be used to enhance the efficacy of MPPα-PDT.

Cyclin-dependent kinase inhibitor (p21; CDKI) is a target gene encoded by ATF4 and plays a role in promoting cell survival under ER stress. Here, the ChIP assay revealed that p21 intron 1 bears ATF4-responsive elements that bind to ATF4. ATF4 silencing suppressed p21 expression levels after MPPα-PDT treatment, consistent with past findings [20, 41]. Our findings confirm the pro-survival role of p21, which could be suppressed by PERK signaling inhibition. P21 expression was increased by elevated ATF4 under ER stress, whereas p21 silencing enhanced apoptosis after MPPα-PDT treatment in HOS cells. These results indicate a pro-survival role of p21. Furthermore, it has been established that p21 plays a part in autophagy regulation across different cell types. Al and colleagues [42] reported that p21 could influence the creation of LC3-II through direct interaction with LC3. Moreover, the antimalarial medication quinacrine promotes autophagy and apoptosis in breast cancer cells by modulating p21, which consequently inhibits tumor cell proliferation [43]. Hence, targeting p21 could be a means of indirectly regulating autophagy and affecting the anti-tumor ability of MPPα-PDT. Taken together, our findings indicate that PERK-signaling-dependent upregulation of p21 may counteract the pro-apoptotic effects of MPPα-PDT, whereas PERK signaling inhibition may enhance sensitivity to MPPα-PDT.

Meanwhile, there are some limitations to this study such as potential off-target effects or the necessity for further investigations to validate the observed effects, particularly in relation to the p21 pro-survival findings. Additionally, traditional PDT strategies have primarily focused on treating superficial cancers due to their non-invasive nature, high selectivity, and minimal side effects. The clinical application of PDT is currently limited to peripheral and endoscopically accessible areas (such as skin, neck, and mouth). However, the effectiveness of therapy for deep tumors is hindered by the limited tissue penetration depth of excitation light and poor *in vivo* targeting of photosensitizers.

In conclusion (Figure 9), we sought to better understand how PERK signaling promotes the HOS cell survival induced by MPPα-PDT, as overcoming this may enhance sensitivity to MPPα-PDT. We found that MPPα-PDT combined with GSK2656157 enhances HOS cell apoptosis by suppressing autophagy. Crucially, this autophagy is p21-dependent, also indicating a pro-survival role of p21 during MPPα-PDT treatment. As inhibition of PERK signaling with GSK2656157 had similar results, it is possible that in the combined treatment group, GSK2656157 overcame p21-dependent autophagy to enhance HOS cells' sensitivity to MPPα-PDT *in vivo* and *in vitro*.

AUTHOR CONTRIBUTIONS

Conceptualization, Shenxi Zhong; Formal analysis, Ye Zhang and Changchun Jian; Funding acquisition, Ye Zhang and Yunsheng Ou; Methodology, Ye Zhang and Hai Mou; Supervision, Yunsheng Ou; Validation, Shenxi Zhong and Ye Zhang; Visualization, Shenxi Zhong and Yunsheng Ou; Writing – Original draft, Shenxi Zhong, Ye Zhang and Qiu Huang.

CONFLICTS OF INTEREST

The authors declare no conflicts of interest related to this study.

ETHICAL STATEMENT

The research protocol was approved by the Ethics Committee of the First Affiliated Hospital of Chongqing Medical University (2022 Scientific Research No. 2022-72). Animal experiments have been reviewed by the Ethics Committee of the First Affiliated Hospital of Chongqing Medical University and meet the requirements of animal ethics and welfare.

FUNDING

This work was supported by the National Natural Science Foundation of China (No. 82172682, No. 82373221); Chongqing Science and Technology Commission (No. CSTB2023NSCQ-MSX0472); 2022 First-class Discipline Construction Project of the First Affiliated Hospital of Chongqing Medical University (No. CYYY-BSYJSCXXM-202207); 2023 First-class Discipline Construction Project of the First Affiliated Hospital of Chongqing Medical University (No. CYYY-BSYJSCXXM-202304).

REFERENCES

1. Whelan JS, Davis LE. Osteosarcoma, Chondrosarcoma, and Chordoma. J Clin Oncol. 2018; 36:188–93. https://doi.org/10.1200/JCO.2017.75.1743 PMID:29220289

2. Bielack SS, Kempf-Bielack B, Branscheid D, Carrle D, Friedel G, Helmke K, Kevric M, Jundt G, Kühne T, Maas R, Schwarz R, Zoubek A, Jürgens H. Second and subsequent recurrences of osteosarcoma: presentation, treatment, and outcomes of 249 consecutive cooperative osteosarcoma study group patients. J Clin Oncol. 2009; 27:557–65. https://doi.org/10.1200/JCO.2008.16.2305 PMID:19075282

3. Smeland S, Bielack SS, Whelan J, Bernstein M, Hogendoorn P, Krailo MD, Gorlick R, Janeway KA, Ingleby FC, Anninga J, Antal I, Arndt C, Brown KLB, et al. Survival and prognosis with osteosarcoma: outcomes in more than 2000 patients in the EURAMOS-1 (European and American Osteosarcoma Study) cohort. Eur J Cancer. 2019; 109:36–50. https://doi.org/10.1016/j.ejca.2018.11.027 PMID:30685685

4. Pham TC, Nguyen VN, Choi Y, Lee S, Yoon J. Recent Strategies to Develop Innovative Photosensitizers for Enhanced Photodynamic Therapy. Chem Rev. 2021; 121:13454–619. https://doi.org/10.1021/acs.chemrev.1c00381 PMID:34582186

5. Mishchenko T, Balalaeva I, Gorokhova A, Vedunova M, Krysko DV. Which cell death modality wins the contest for photodynamic therapy of cancer? Cell Death Dis. 2022; 13:455. https://doi.org/10.1038/s41419-022-04851-4 PMID:35562364

6. Luo T, Wilson BC, Lu QB. Evaluation of one- and two-photon activated photodynamic therapy with pyropheophorbide-a methyl ester in human cervical, lung and ovarian cancer cells. J Photochem Photobiol B. 2014; 132:102–10. https://doi.org/10.1016/j.jphotobiol.2014.02.002 PMID:24607610

7. Huang Q, Ou YS, Tao Y, Yin H, Tu PH. Apoptosis and autophagy induced by pyropheophorbide-α methyl ester-mediated photodynamic therapy in human osteosarcoma MG-63 cells. Apoptosis. 2016; 21:749–60. https://doi.org/10.1007/s10495-016-1243-4 PMID:27108344

8. Tu PH, Huang WJ, Wu ZL, Peng QZ, Xie ZB, Bao J, Zhong MH. Induction of cell death by pyropheophorbide-α methyl ester-mediated photodynamic therapy in lung cancer A549 cells. Cancer Med. 2017; 6:631–9. https://doi.org/10.1002/cam4.1012 PMID:28181425

9. Zhu J, Tian S, Li KT, Chen Q, Jiang Y, Lin HD, Yu LH, Bai DQ. Inhibition of breast cancer cell growth by methyl pyropheophenylchlorin photodynamic therapy is mediated though endoplasmic reticulum stress-induced autophagy in vitro and vivo. Cancer Med. 2018; 7:1908–20. https://doi.org/10.1002/cam4.1418 PMID:29577663

10. Zhan F, He T, Chen Z, Zuo Q, Wang Y, Li Q, Zhong S, Ou Y. RhoA enhances osteosarcoma resistance to MPPa-PDT via the Hippo/YAP signaling pathway. Cell Biosci. 2021; 11:179. https://doi.org/10.1186/s13578-021-00690-6 PMID:34627383

11. Tao Y, Ou Y, Yin H, Chen Y, Zhong S, Gao Y, Zhao Z, He B, Huang Q, Deng Q. Establishment and characterization of human osteosarcoma cells resistant to pyropheophorbide-α methyl ester-mediated photodynamic therapy. Int J Oncol. 2017; 51:1427–38. https://doi.org/10.3892/ijo.2017.4136 PMID:29048645

12. Chakraborty P, Parikh RY, Choi S, Tran D, Gooz M, Hedley ZT, Kim DS, Pytel D, Kang I, Nadig SN, Beeson GC, Ball L, Mehrotra M, et al. Carbon Monoxide Activates PERK-Regulated Autophagy to Induce Immunometabolic Reprogramming and Boost

Antitumor T-cell Function. Cancer Res. 2022; 82:1969–90.
https://doi.org/10.1158/0008-5472.CAN-21-3155
PMID:35404405

13. Xu K, Han B, Bai Y, Ma XY, Ji ZN, Xiong Y, Miao SK, Zhang YY, Zhou LM. MiR-451a suppressing BAP31 can inhibit proliferation and increase apoptosis through inducing ER stress in colorectal cancer. Cell Death Dis. 2019; 10:152.
https://doi.org/10.1038/s41419-019-1403-x
PMID:30770794

14. Eizirik DL, Miani M, Cardozo AK. Signalling danger: endoplasmic reticulum stress and the unfolded protein response in pancreatic islet inflammation. Diabetologia. 2013; 56:234–41.
https://doi.org/10.1007/s00125-012-2762-3
PMID:23132339

15. Hosomi S, Grootjans J, Huang YH, Kaser A, Blumberg RS. New Insights Into the Regulation of Natural-Killer Group 2 Member D (NKG2D) and NKG2D-Ligands: Endoplasmic Reticulum Stress and CEA-Related Cell Adhesion Molecule 1. Front Immunol. 2018; 9:1324.
https://doi.org/10.3389/fimmu.2018.01324
PMID:29973929

16. Jang JE, Eom JI, Jeung HK, Chung H, Kim YR, Kim JS, Cheong JW, Min YH. PERK/NRF2 and autophagy form a resistance mechanism against G9a inhibition in leukemia stem cells. J Exp Clin Cancer Res. 2020; 39:66.
https://doi.org/10.1186/s13046-020-01565-3
PMID:32293500

17. Kim SM, Ha SE, Lee HJ, Rampogu S, Vetrivel P, Kim HH, Venkatarame Gowda Saralamma V, Lee KW, Kim GS. Sinensetin Induces Autophagic Cell Death through p53-Related AMPK/mTOR Signaling in Hepatocellular Carcinoma HepG2 Cells. Nutrients. 2020; 12:2462.
https://doi.org/10.3390/nu12082462
PMID:32824273

18. Ding H, Song Y, Huang X, Wang L, Luo S, Zhang H, Pan H, Jiang W, Qian J, Yao G, Wen L, Zhang Y. mTORC1-dependent TFEB nucleus translocation and pro-survival autophagy induced by zeolitic imidazolate framework-8. Biomater Sci. 2020; 8:4358–69.
https://doi.org/10.1039/d0bm00773k
PMID:32608399

19. Chen Y, Yin H, Tao Y, Zhong S, Yu H, Li J, Bai Z, Ou Y. Antitumor effects and mechanisms of pyropheophorbide-α methyl ester-mediated photodynamic therapy on the human osteosarcoma cell line MG-63. Int J Mol Med. 2020; 45:971–82.
https://doi.org/10.3892/ijmm.2020.4494
PMID:32124948

20. Inoue Y, Kawachi S, Ohkubo T, Nagasaka M, Ito S, Fukuura K, Itoh Y, Ohoka N, Morishita D, Hayashi H. The CDK inhibitor p21 is a novel target gene of ATF4 and contributes to cell survival under ER stress. FEBS Lett. 2017; 591:3682–91.
https://doi.org/10.1002/1873-3468.12869
PMID:28975618

21. Ohoka N, Yoshii S, Hattori T, Onozaki K, Hayashi H. TRB3, a novel ER stress-inducible gene, is induced via ATF4-CHOP pathway and is involved in cell death. EMBO J. 2005; 24:1243–55.
https://doi.org/10.1038/sj.emboj.7600596
PMID:15775988

22. Atkins C, Liu Q, Minthorn E, Zhang SY, Figueroa DJ, Moss K, Stanley TB, Sanders B, Goetz A, Gaul N, Choudhry AE, Alsaid H, Jucker BM, et al. Characterization of a novel PERK kinase inhibitor with antitumor and antiangiogenic activity. Cancer Res. 2013; 73:1993–2002.
https://doi.org/10.1158/0008-5472.CAN-12-3109
PMID:23333938

23. Kim C, Davis LE, Albert CM, Samuels B, Roberts JL, Wagner MJ. Osteosarcoma in Pediatric and Adult Populations: Are Adults Just Big Kids? Cancers (Basel). 2023; 15:5044.
https://doi.org/10.3390/cancers15205044
PMID:37894411

24. Poos K, Smida J, Maugg D, Eckstein G, Baumhoer D, Nathrath M, Korsching E. Genomic heterogeneity of osteosarcoma - shift from single candidates to functional modules. PLoS One. 2015; 10:e0123082.
https://doi.org/10.1371/journal.pone.0123082
PMID:25848766

25. Olivos DJ, Mayo LD. Emerging Non-Canonical Functions and Regulation by p53: p53 and Stemness. Int J Mol Sci. 2016; 17:1982.
https://doi.org/10.3390/ijms17121982
PMID:27898034

26. Forment JV, Kaidi A, Jackson SP. Chromothripsis and cancer: causes and consequences of chromosome shattering. Nat Rev Cancer. 2012; 12:663–70.
https://doi.org/10.1038/nrc3352
PMID:22972457

27. Rankin EB, Giaccia AJ. The role of hypoxia-inducible factors in tumorigenesis. Cell Death Differ. 2008; 15:678–85.
https://doi.org/10.1038/cdd.2008.21
PMID:18259193

28. Lou J, Jiang L, Dai X, Wang H, Yang J, Guo L, Fang M, Wang S. Radiation-Induced Sarcoma of the Head and Neck Following Radiotherapy for Nasopharyngeal Carcinoma: A Single Institutional

Experience and Literature Review. Front Oncol. 2021; 10:526360.
https://doi.org/10.3389/fonc.2020.526360
PMID:33552942

29. Bacellar IO, Tsubone TM, Pavani C, Baptista MS. Photodynamic Efficiency: From Molecular Photochemistry to Cell Death. Int J Mol Sci. 2015; 16:20523–59.
https://doi.org/10.3390/ijms160920523
PMID:26334268

30. Huang L, Lin H, Chen Q, Yu L, Bai D. MPPa-PDT suppresses breast tumor migration/invasion by inhibiting Akt-NF-κB-dependent MMP-9 expression via ROS. BMC Cancer. 2019; 19:1159.
https://doi.org/10.1186/s12885-019-6374-x
PMID:31783821

31. Tian Y, Leung W, Yue K, Mak N. Cell death induced by MPPa-PDT in prostate carcinoma in vitro and in vivo. Biochem Biophys Res Commun. 2006; 348:413–20.
https://doi.org/10.1016/j.bbrc.2006.07.071
PMID:16889752

32. Marciniak SJ, Chambers JE, Ron D. Pharmacological targeting of endoplasmic reticulum stress in disease. Nat Rev Drug Discov. 2022; 21:115–40.
https://doi.org/10.1038/s41573-021-00320-3
PMID:34702991

33. Odle RI, Walker SA, Oxley D, Kidger AM, Balmanno K, Gilley R, Okkenhaug H, Florey O, Ktistakis NT, Cook SJ. An mTORC1-to-CDK1 Switch Maintains Autophagy Suppression during Mitosis. Mol Cell. 2020; 77:228–40.e7.
https://doi.org/10.1016/j.molcel.2019.10.016
PMID:31733992

34. Kusio-Kobialka M, Podszywalow-Bartnicka P, Peidis P, Glodkowska-Mrowka E, Wolanin K, Leszak G, Seferynska I, Stoklosa T, Koromilas AE, Piwocka K. The PERK-eIF2α phosphorylation arm is a pro-survival pathway of BCR-ABL signaling and confers resistance to imatinib treatment in chronic myeloid leukemia cells. Cell Cycle. 2012; 11:4069–78.
https://doi.org/10.4161/cc.22387
PMID:23095523

35. Zhao A, Zhang Z, Zhou Y, Li X, Li X, Ma B, Zhang Q. β-Elemonic acid inhibits the growth of human Osteosarcoma through endoplasmic reticulum (ER) stress-mediated PERK/eIF2α/ATF4/CHOP activation and Wnt/β-catenin signal suppression. Phytomedicine. 2020; 69:153183.
https://doi.org/10.1016/j.phymed.2020.153183
PMID:32113150

36. Tallóczy Z, Virgin HW 4th, Levine B. PKR-dependent autophagic degradation of herpes simplex virus type 1. Autophagy. 2006; 2:24–9.
https://doi.org/10.4161/auto.2176
PMID:16874088

37. B'chir W, Maurin AC, Carraro V, Averous J, Jousse C, Muranishi Y, Parry L, Stepien G, Fafournoux P, Bruhat A. The eIF2α/ATF4 pathway is essential for stress-induced autophagy gene expression. Nucleic Acids Res. 2013; 41:7683–99.
https://doi.org/10.1093/nar/gkt563
PMID:23804767

38. Ji GR, Yu NC, Xue X, Li ZG. PERK-mediated Autophagy in Osteosarcoma Cells Resists ER Stress-induced Cell Apoptosis. Int J Biol Sci. 2015; 11:803–12.
https://doi.org/10.7150/ijbs.11100
PMID:26078722

39. Zhao C, Yu D, He Z, Bao L, Feng L, Chen L, Liu Z, Hu X, Zhang N, Wang T, Fu Y. Endoplasmic reticulum stress-mediated autophagy activation is involved in cadmium-induced ferroptosis of renal tubular epithelial cells. Free Radic Biol Med. 2021; 175:236–48.
https://doi.org/10.1016/j.freeradbiomed.2021.09.008
PMID:34520822

40. Chen D, Fan Z, Rauh M, Buchfelder M, Eyupoglu IY, Savaskan N. ATF4 promotes angiogenesis and neuronal cell death and confers ferroptosis in a xCT-dependent manner. Oncogene. 2017; 36:5593–608.
https://doi.org/10.1038/onc.2017.146
PMID:28553953

41. Ebert SM, Monteys AM, Fox DK, Bongers KS, Shields BE, Malmberg SE, Davidson BL, Suneja M, Adams CM. The transcription factor ATF4 promotes skeletal myofiber atrophy during fasting. Mol Endocrinol. 2010; 24:790–9.
https://doi.org/10.1210/me.2009-0345
PMID:20197309

42. Al Bitar S, Gali-Muhtasib H. The Role of the Cyclin Dependent Kinase Inhibitor $p21^{cip1/waf1}$ in Targeting Cancer: Molecular Mechanisms and Novel Therapeutics. Cancers (Basel). 2019; 11:1475.
https://doi.org/10.3390/cancers11101475
PMID:31575057

43. Hwang JR, Kim WY, Cho YJ, Ryu JY, Choi JJ, Jeong SY, Kim MS, Kim JH, Paik ES, Lee YY, Han HD, Lee JW. Chloroquine reverses chemoresistance via upregulation of p21(WAF1/CIP1) and autophagy inhibition in ovarian cancer. Cell Death Dis. 2020; 11:1034.
https://doi.org/10.1038/s41419-020-03242-x
PMID:33277461

SUPPLEMENTARY MATERIALS

Supplementary Figures

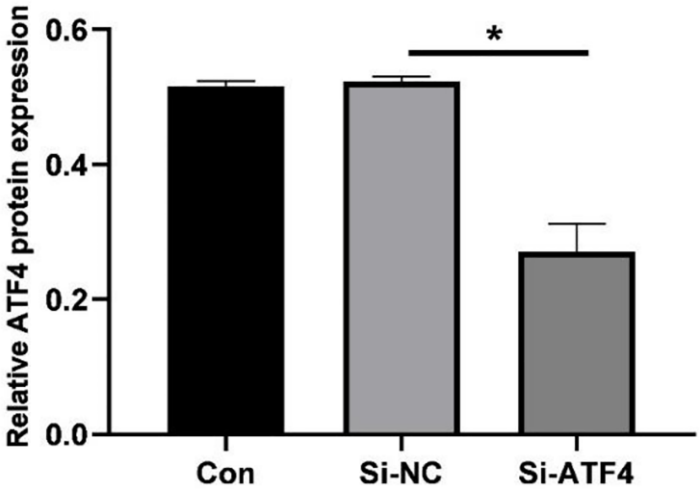

Supplementary Figure 1. Relative ATF4 protein expression.

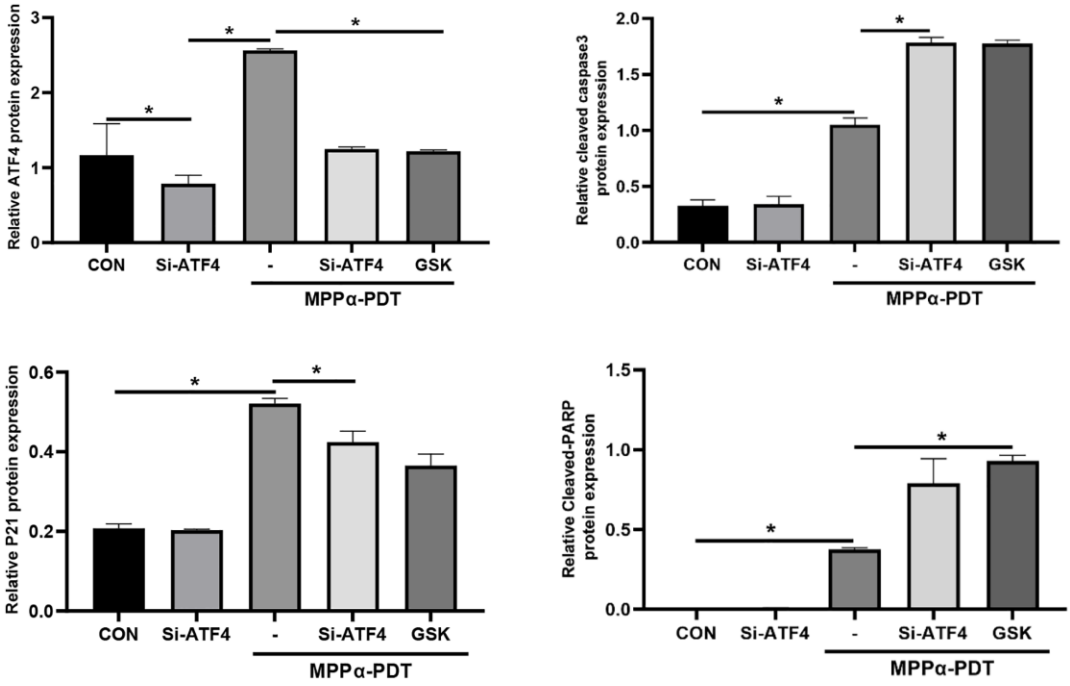

Supplementary Figure 2. Relative P21, cleaved-caspase3, ATF4, PARP proteins expression.

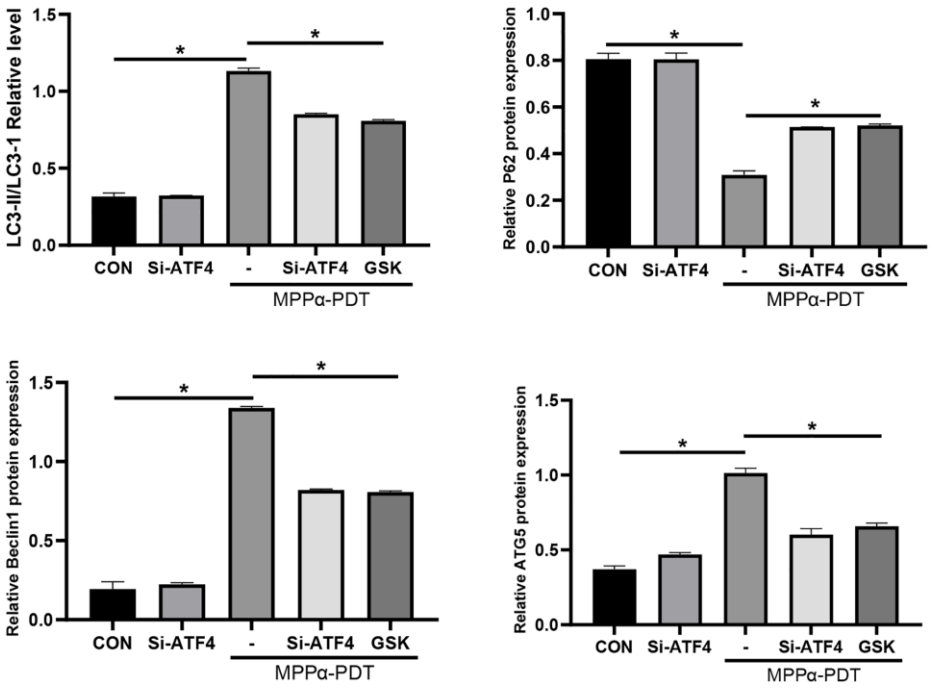

Supplementary Figure 3. Relative ATG5, P62, LC3II/LC3I, Beclin1 proteins expression.

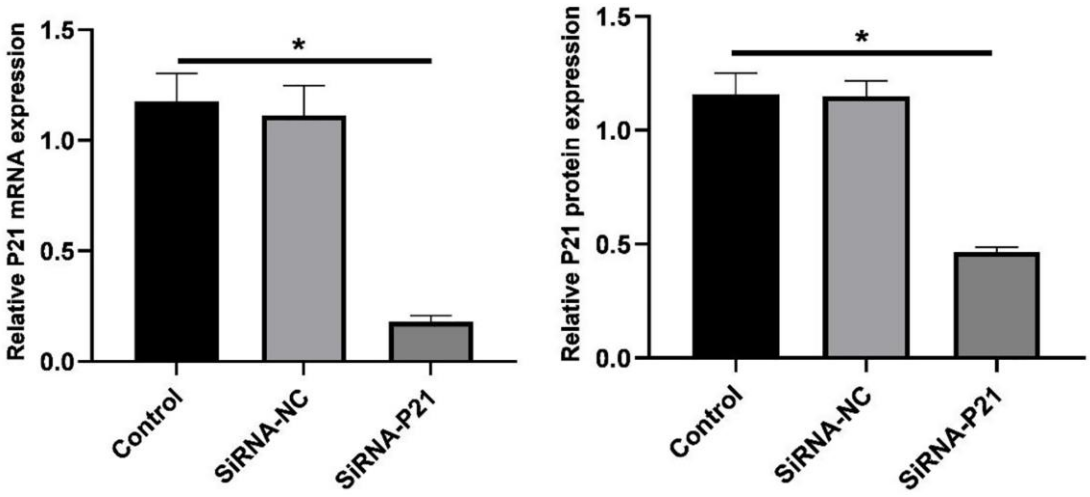

Supplementary Figure 4. Relative P21 protein expression and P21 mRNA expression.

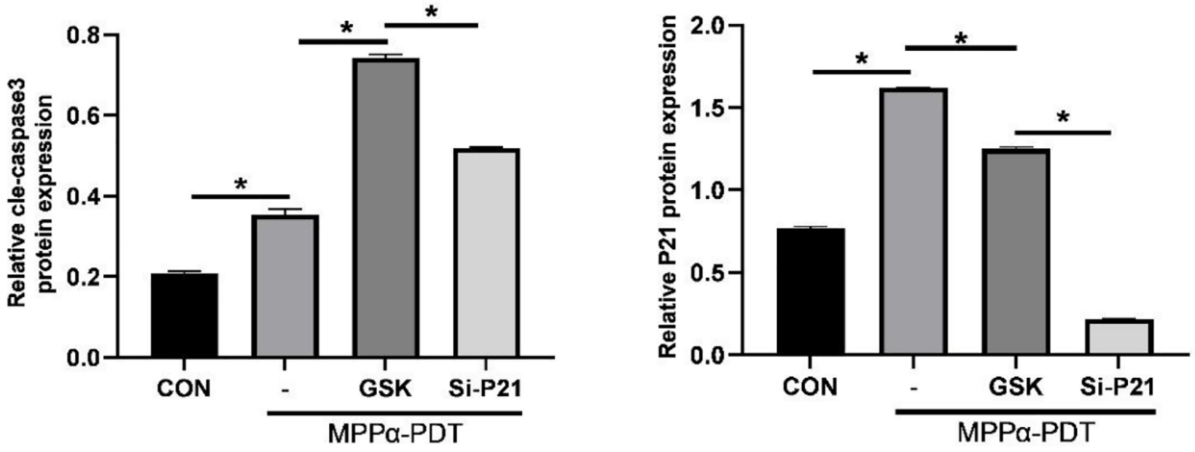

Supplementary Figure 5. Relative cleaved-caspase3 and p21 proteins expression.

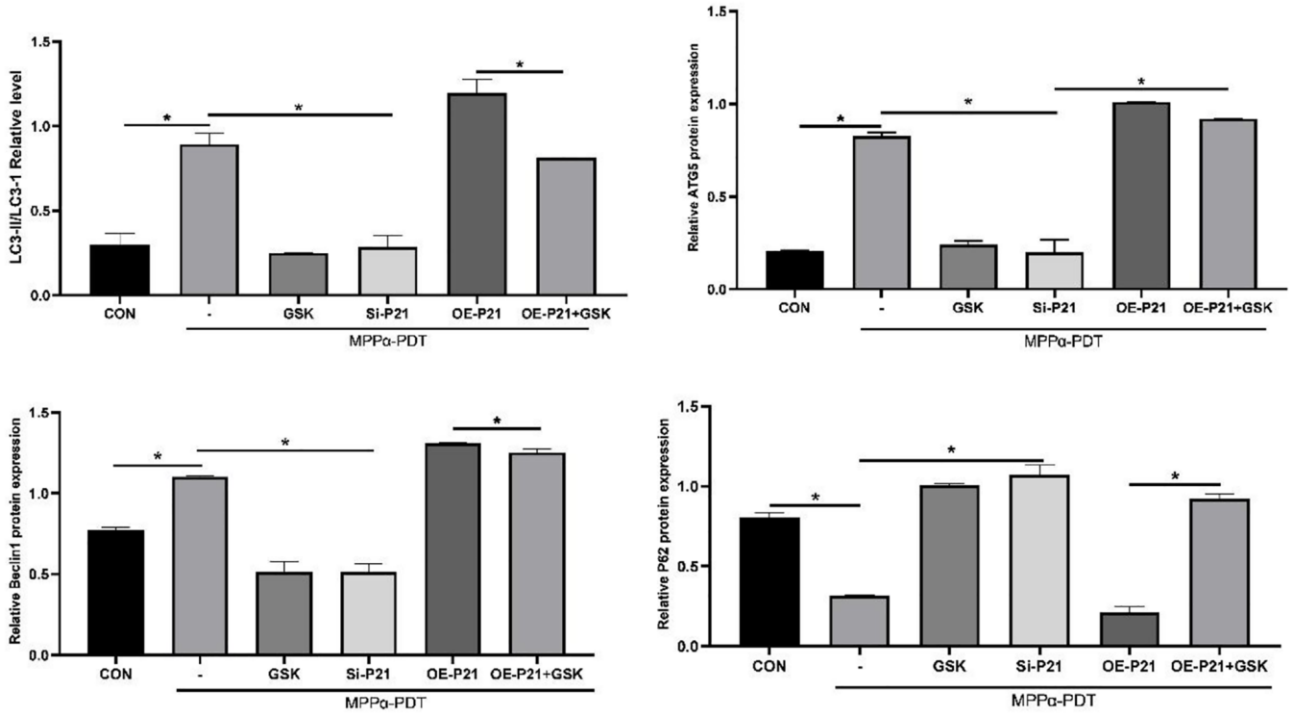

Supplementary Figure 6. Relative LC3II/LC3I, ATG5, Beclin1, P62 proteins expression.

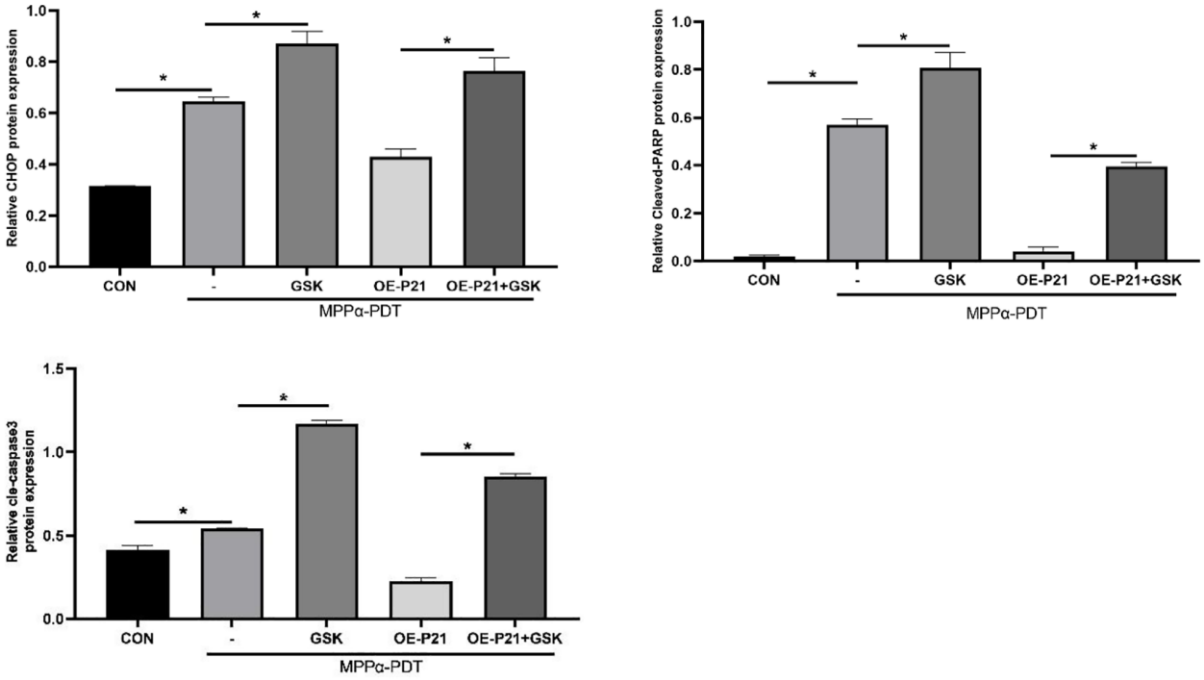

Supplementary Figure 7. Relative CHOP, cleaved-caspase3, cleaved-PARP proteins expression.